Identification of Highly Reactive Positions in the Antibody Lambda Light-Chain for Efficient Chemical Conjugation Using Expanded Genetic Code

加藤, 明文

Doctoral Dissertation

Identification of Highly Reactive Positions in the Antibody Lambda Light Chain for Efficient Chemical Conjugation Using Expanded Genetic Code

November 2020

Department of Pharmaceutical Cell Biology

Graduate School of Pharmaceutical Sciences

Kyushu University

Akifumi Kato

Table of Contents

Abbreviations

ADC	antibody-drug conjugate
ADCC	antibody-dependent cellular cytotoxicity
ASA	solvent-accessible surface area
BCR	B-cell receptor
CDC	complement-dependent cytotoxicity
CH1	first constant region of the heavy chain
Cix	cixutumumab
CLκ	κ light chain constant region
CLλ	λ light chain constant region
CPK	Corey-Pauling-Koltun
DARPin	designed ankyrin repeat protein
DBCO	dibenzylcyclooctyne
EGFR	epidermal growth factor receptor
ELISA	enzyme-linked immunosorbent assay
EPO	erythropoietin
Fab	antigen-binding fragment
FBS	fetal bovine serum
FcγR	Fcγ receptor
FDA	Food and Drug Administration
FGF21	fibroblast growth factor 21
FGFR1C	fibroblast growth factor receptor 1C
FZD	frizzled
GST	glutathione S-transferase

HC	heavy chain
HER2	human epidermal growth factor receptor 2
His	histidine
HPLC	high-performance liquid chromatography
HRP	horseradish peroxidase
Ig	immunoglobulin
IGF1	insulin-like growth factor 1
IGF1R	insulin-like growth factor-1 receptor
JAK2	Janus kinase 2
KLB	β-klotho
LC	light chain
LC-MS	liquid chromatography–mass spectrometry
MMAE	monomethyl auristatin E
nnAA	non-natural amino acid
o-Az-Z-Lys	Nε-(*o*-Azidobenzyloxycarbonyl)-L-lysine
OI	optical imaging
p-AcF	*p*-acetophenylalanine
p-AzF	*p*-azidophenylalanine
PBS	phosphate-buffered saline
PCR	polymerase chain reaction
PDB	Protein Data Bank
PEG	polyethylene glycol
PET	positron emission tomography
PylRS	pyrrolysyl-tRNA synthetase

RF-1	release factor-1
SDS-PAGE	sodium dodecyl sulfate polyacrylamide gel electrophoresis
SPAAC	strain-promoted alkyne-azide cycloaddition
TBST	tris-buffered saline containing 0.05% tween-20
T_m	melting temperature
Tra	trastuzumab
VL	light chain variable region
Z-Lys	Nε-benzyloxycarbonyl-L-lysine

1 Abstract

Site-specific chemical conjugation of antibodies using genetically incorporated non-natural amino acids (nnAAs) shows promise to advance antibody-drug conjugates (ADCs) and create bispecific antibodies. Most of the current approved therapeutic antibodies are immunoglobulin G kappa (IgGκ) isotypes, and antibody engineering through nnAA incorporation has mainly focused on IgGκ, whereas IgG lambda (λ) has relatively not been explored yet. In this study, we applied the codon-reassignment technology to achieve robust and efficient synthesis of chemically functionalized antigen-binding fragments (Fabs) derived from IgGλ containing Nε-(*o*-azidobenzyloxycarbonyl)-L-lysine (*o*-Az-Z-Lys) at defined positions. This lysine derivative has a bio-orthogonally reactive group at the end of a long side chain, enabling identification of multiple positions in λ light chain constant regions (CLλs) with high conjugation efficiency and allowing the preparation of Fab-drug conjugates and antagonistic bispecific Fab-dimers in cultured cells. These results show that our approach greatly enhanced the availability of antibodies that have CLλ constant domains for chemical conjugation and might aid in the development of novel therapeutic antibodies.

2 Introduction

Immunoglobulins (Igs) are highly specific molecules that can bind with high affinity to their cognate antigens and participate in immunological defense as a result of the activation of their effector functions, including complement-dependent cytotoxicity (CDC), phagocytosis, and antibody-dependent cellular cytotoxicity (ADCC). Igs are classified into five classes according to the constant region of their heavy chains (HCs): IgA, IgD, IgE, IgG, and IgM antibodies. IgGs are hetero-tetrameric proteins composed of two identical IgG HCs and two identical light chains (LCs) [1, 2]. The LC genes are encoded by two separate loci, subdividing the entity of antibodies into kappa (LCκ) and lambda (LCλ) isotypes. LCκ and LCλ exhibit distinct sequence (Figure 1) and conformational properties characterized by the disulfide bond susceptibility to reducing conditions [3-5].

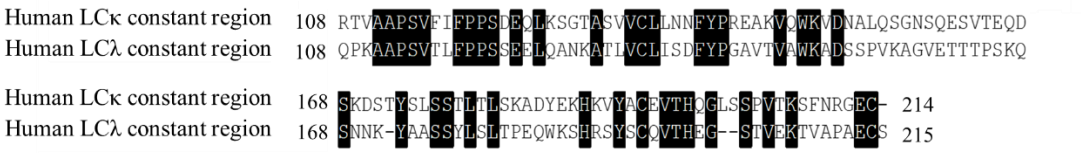

Figure 1. Sequence similarity of human LCκ and LCλ constant regions.

The matched amino acid residues are highlighted in black. The sequence information was obtained from trastuzumab (a humanized IgG1κ antibody) and cixutumumab (a humanized IgG1λ antibody) [6, 7].

Ig, immunoglobulin; LC, light chain.

For intact Igs, the κ to λ ratio is roughly 2:1 in serum [8]. IgGs, being well-studied and with a stable structure, are commonly used as therapeutics. More than 70 antibodies have been approved by the United States Food and Drug Administration (FDA), and most of them belong to the human IgG isotype [9]. Among the approved IgGs, IgGκ, which possesses the κ LC constant region (CLκ), is dominant, whereas only six antibodies possess the λ LC constant region (CLλ) [9]. This bias toward the κ isotype is likely because most of these antibodies are chimeric or humanized derivatives of antibodies generated from rodents. The ratio of IgGκ to IgGλ isoforms is 19:1 in the serum of mouse [8], the most commonly immunized organism for antibody acquisition. With advances in human phage display libraries containing more balanced κ to λ ratios and human B-cell cloning technology, more human IgGλ isotype antibodies have been identified in preclinical programs and are entering clinical pipelines. Antibody engineering, including site-specific conjugation, has been applied to generate antibody-based therapeutics, such as antibody-drug conjugates (ADCs) and bispecific antibodies, with a focus mainly on the HC and CLκ of IgGs [10-20]; however, not much information has been obtained on CLλ.

Genetic incorporation of non-natural amino acids (nnAAs) into antibodies using expanded genetic codes guarantees site specificity. Small molecules, fluorescent probes, peptides, polyethylene glycol (PEG), and proteins can be conjugated to antibodies through bio-orthogonal chemical reactions involving these nnAAs. IgG antibodies have been conjugated to anticancer drugs [17, 18, 21, 22], whereas antigen-binding fragments (Fabs) have been transformed into bispecific antibodies [19, 20]. Several techniques can be used to modify proteins site-specifically. For example, cysteine is a reactive “natural” amino acid; however, engineered cysteines

coupled through maleimide chemistry can be reversible and unstable [23], which are important limitations for antibody engineering of ADCs and bispecific antibodies. Therefore, the stable and selective bio-orthogonal conjugation strategy using nnAAs provides a powerful approach to generate ADCs and to manipulate and investigate the structure and function of bispecific antibodies.

The precise design of conjugates has been achieved by the definition of conjugation sites in antibody molecules through assigning specific codons such as the amber stop codon (UAG) to nnAAs [24]. The competition between UAG-translating tRNAs and Release Factor-1 (RF-1), the release factor recognizing UAG for termination of protein synthesis, results in variations in incorporation efficiency depending on the sequence surrounding the UAG codon [25]. This vulnerability, termed "sequence context," prevents a comprehensive survey of useful conjugation sites within the antibody. Therefore, RF-1–knockout cells, which can avoid sequence context, are expected to be better hosts for incorporating nnAAs into antibodies (Figure 2). RF-1, previously thought to be an essential cellular factor, can be eliminated with no significant reduction in bacterial protein productivity if some or all the genes ending with the UAG codon are engineered to end with other stop codons [26-30]. Because RF-1 confers stop-codon status to the codon, in its absence, UAG is redefined to represent any amino acid according to the amino acid specificity of UAG-recognizing tRNAs (Figure 2). With a guaranteed efficient and robust UAG translation, the selection of nnAAs is important for achieving efficient conjugation.

A) Wild-type *E. coli*

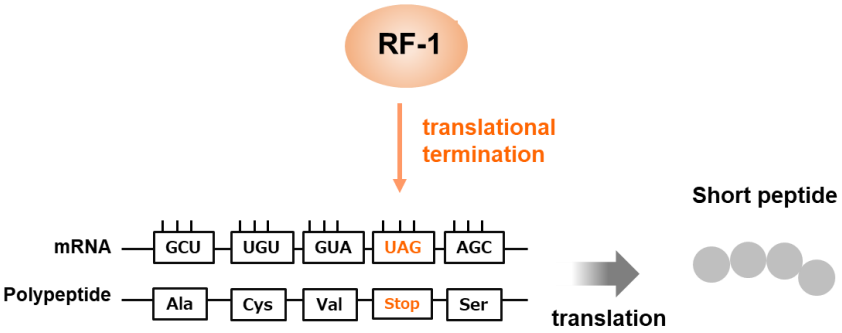

B) Conventional method of nnAA incorporation using wild-type *E. coli.*

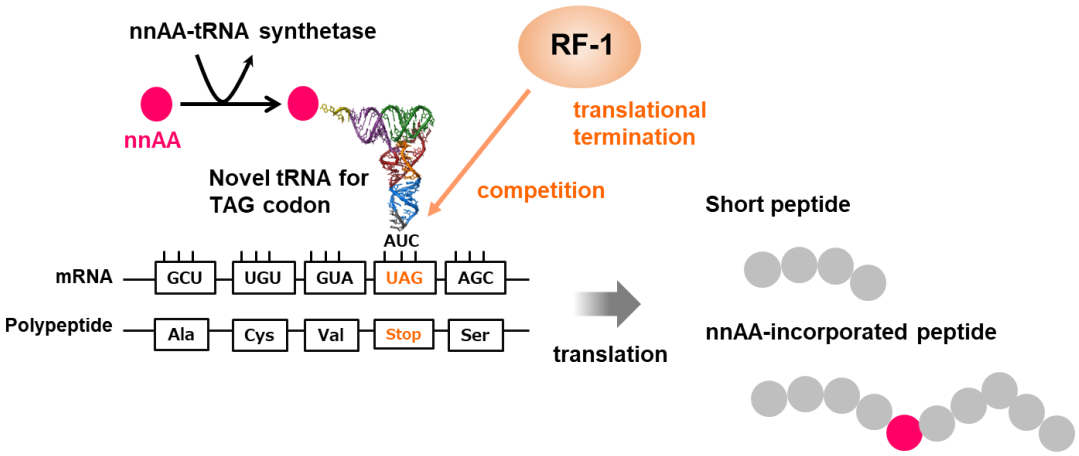

C) Novel method of nnAA incorporation using " RF-1-kockout *E. coli.*"

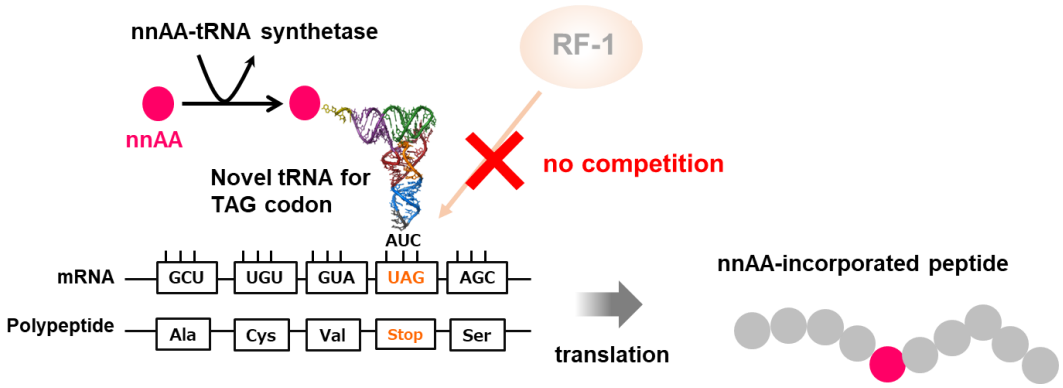

Figure 2. An overview of the system of nnAA incorporation into proteins.

(A) The wild-type *E. coli* translational system, the basic translation machinery, tRNA, mRNA, and the growing polypeptide are shown. A tRNA charged with its cognate amino acid recognizes its specific codon in the mRNA and transfers its amino acid to the growing translation product. The UAG amber stop codon is recognized by RF-1 and the translation is terminated.

(B) The conventional method of nnAA incorporation using wild-type *E. coli* cells. nnAA-tRNA synthetase and a novel tRNA that recognizes the TAG amber codon were introduced. nnAA-tRNA synthetase aminoacylates its cognate tRNA with a specific nnAA (red circle). These cellular machineries can incorporate an nnAA into a growing peptide chain. The introduced tRNA competes with RF-1, and this results in the restriction of the translational efficiency and protein productivity.

(C) Using the RF-1–knockout *E.coli* strain [6], complete reassignment of the UAG amber stop codon to a sense codon of an nnAA was achieved by the elimination of RF-1.

nnAA, non-natural amino acid; RF-1, Release Factor-1.

While over 50 nnAAs have been genetically incorporated into recombinant proteins, those most widely used for producing bioconjugates are *p*-acetophenylalanine (*p*-AcF), *p*-azidophenylalanine (*p*-AzF), and pyrrolysine derivatives [31, 32]. Most organisms use only the 20 common natural amino acids as building blocks for proteins; however, certain archaebacteria incorporate pyrrolysine and selenocysteine as the 21st and 22nd natural amino acids [33]. Pyrrolysine derivatives can contain reactive groups at the end of a long side chain, thereby largely increasing the solvent

exposure of these groups (Figure 3) [34]. *Nε*-(*o*-Azidobenzyloxycarbonyl)-L-lysine (*o*-Az-Z-Lys) contains an azido group located 13 Å away from the Cα atom, whereas *p*-AzF positions the group much closer (7 Å) to the main-chain atom [35]. This difference highlights an advantage of using *o*-Az-Z-Lys for chemical conjugation by bio-orthogonal, selective, and rapid reactions such as strain-promoted alkyne-azide cycloaddition (SPAAC) with dibenzylcyclooctyne (DBCO) (Figure 4) [36].

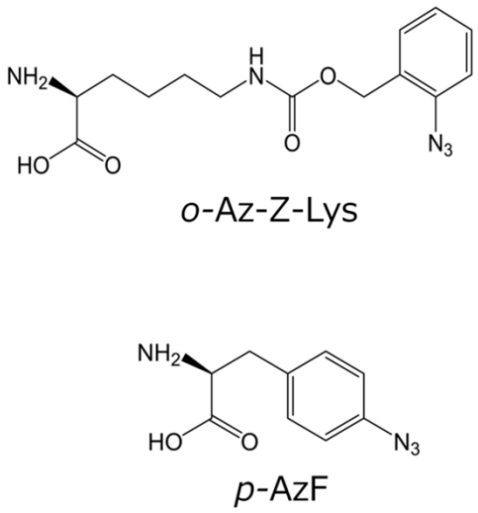

Figure 3. Chemical structures of *o*-Az-Z-Lys and *p*-AzF.

o-Az-Z-Lys, *Nε*-(*o*-Azidobenzyloxycarbonyl)-L-lysine; *p*-AzF, *p*-azidophenylalanine.

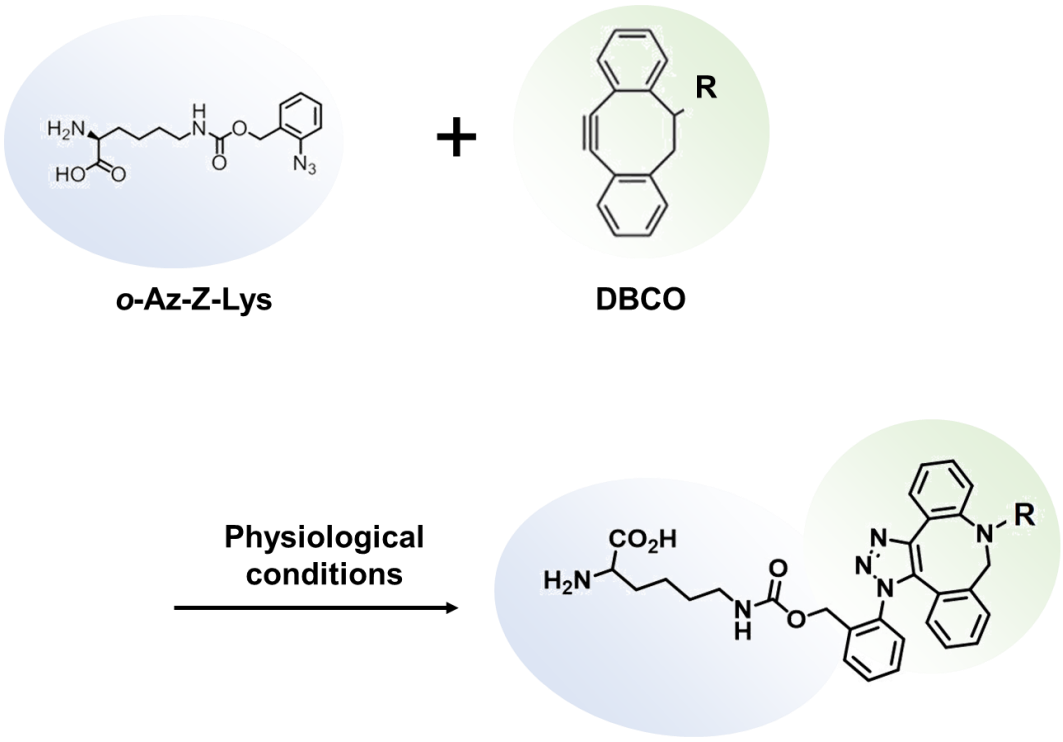

Figure 4. Schematic image of SPAAC between *o*-Az-Z-Lys and DBCO.

DBCO, dibenzylcyclooctyne; *o*-Az-Z-Lys, *N*ε-(*o*-Azidobenzyloxycarbonyl)-L-lysine; SPAAC, strain-promoted alkyne-azide cycloaddition.

Incorporation of nnAAs into proteins can be achieved via the UAG codon and "orthogonal" tRNA/aminoacyl tRNA synthetase pair, which do not cross-react with the host counterparts (Figure 2) [37, 38]. Pyrrolysine is directly esterified to its specific tRNA ($tRNA^{Pyl}$), which has the anticodon (CUA) complementary to the UAG codon, by pyrrolysyl-tRNA synthetase (PylRS) [39, 40]. Besides pyrrolysine, several non-natural pyrrolysine/lysine derivatives are esterified to $tRNA^{Pyl}$ by PylRS. By using PylRS and $tRNA^{Pyl}$ in *E. coli*, some of these non-natural pyrrolysine/lysine derivatives are incorporated into proteins in response to the amber codon [40]. In

order to expand the range of nnAAs that can be incorporated into proteins, such as bulky lysine derivatives like *o*-Az-Z-Lys, Yanagisawa et al identified a structure-based mutant of *Methanosarcina mazei (M. mazei)* PylRS with Y306A and Y384F, which has an expanded amino acid–binding pocket enabling efficient recognition and site-specific incorporation of *o*-Az-Z-Lys into proteins [34].

In our previous study, we assigned UAG to *o*-Az-Z-Lys in an RF-1–knockout *E. coli* W3110 strain and synthesized variants of a Fab fragment containing *o*-Az-Z-Lys at different positions. The constant regions of the antibody, CLκ and CH1 (first constant region of the HC), were extensively explored, resulting in the discovery of multiple novel positions supporting efficient conjugation (Figure 5).

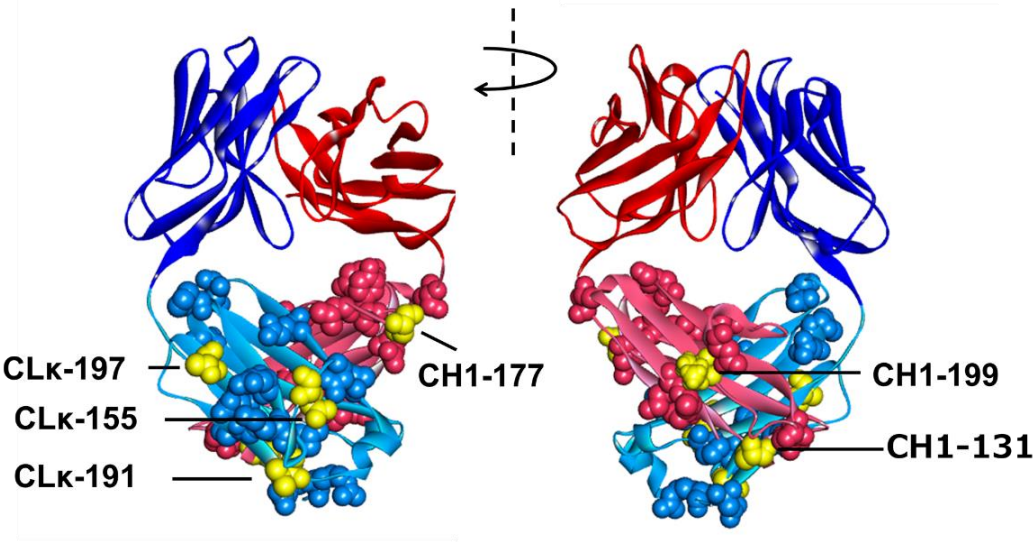

Figure 5. Locations of the selected positions in the tertiary structure of a representative CLκ Fab.

Trastuzumab-Fab, showing the heavy (red) and light (blue) chains in ribbon format and positions of the amino acids (CPK format) that were individually mutated in separate constructs to encode *o*-Az-Z-Lys. The positions that showed high SPAAC reactivity (>90%) and the six representative positions are colored in yellow. Structures are derived from a reported crystal structure (PDB ID: 1N8Z).

CH1, first constant region of the heavy chain; CLκ, κ light chain constant region; CPK, Corey-Pauling-Koltun; Fab, antigen-binding fragment; *o*-Az-Z-Lys, *N*ε-(*o*-Azidobenzyloxycarbonyl)-L-lysine; PDB, Protein Data Bank; SPAAC, strain-promoted alkyne-azide cycloaddition.

Subsequently, we developed a combinatorial platform for producing novel monospecific and bispecific Fab-dimers in a one-pot manner allowing various connections between two Fab molecules (Figure 6). Based on this system, we prepared a wide variety of Fab-dimers using six representative positions with varying relative spatial arrangements between the two Fabs. Some of the created Fab-dimers exhibited agonistic activity in cultured cells as opposed to the antagonistic nature of antibodies. These results showed that the reorientation of Fab domains of antibodies by chemical linkage profoundly converts their biological activities.

In this study, we expanded the previous extensive survey of CLλ and identified multiple novel positions supporting efficient *o*-Az-Z-Lys incorporation and chemical conjugation. These positions allow generation of Fab-drug conjugates and bispecific Fab-dimers and show a promising strategy for engineering more effective antibody-based therapeutics.

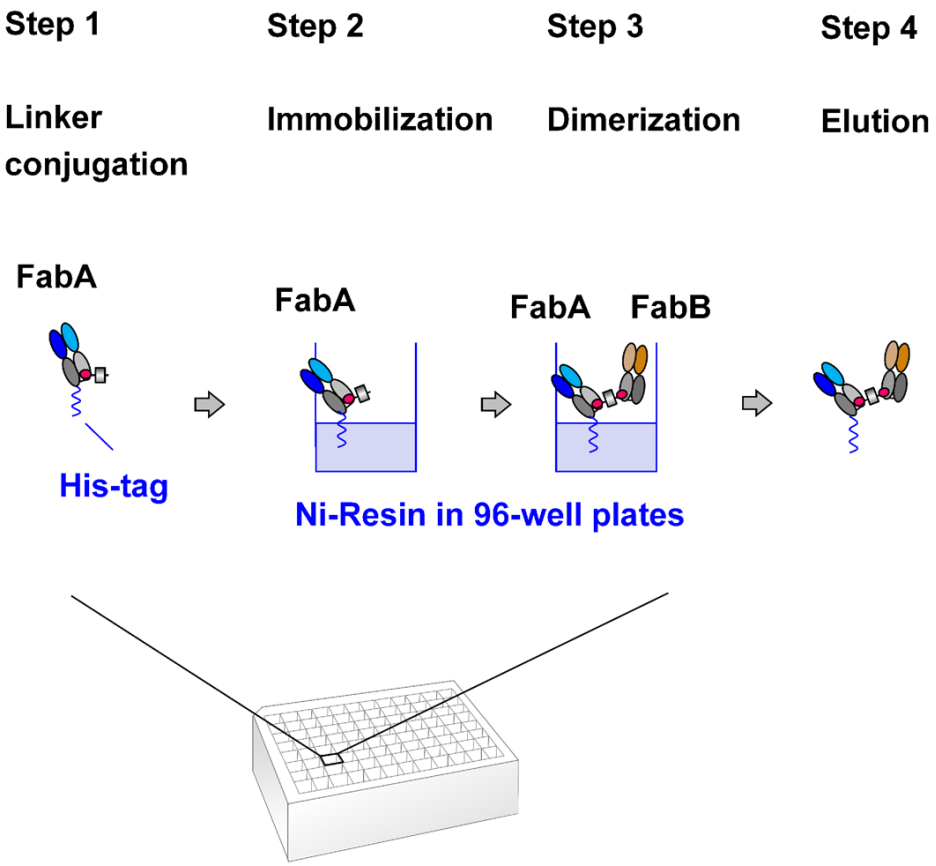

Figure 6. Schematic image of one-pot preparation of bispecific Fab-dimers using a 96-well filter plate filled with an Ni resin.

Fab containing *o*-Az-Z-Lys (Fab A) was conjugated with a linker (step 1) and then immobilized on a Ni resin via a hexa-His tag (step 2), followed by conjugation with another Fab containing *o*-Az-Z-Lys (Fab B) and no tag (step 3) and retrieval of the Fab-dimer by elution using an imidazole buffer (step 4).

Fab, antigen-binding fragment; His, histidine; *o*-Az-Z-Lys, *N*ε-(*o*-Azidobenzyloxycarbonyl)-L-lysine.

3 Materials and Methods

3.1 Materials

o-Az-Z-Lys was purchased from GVK Biosciences (Hyderabad, India). Nε-benzyloxycarbonyl-L-lysine (Z-Lys) was obtained from BachemAG (Bubendorf, Switzerland). DIBO-Alexa Fluor 488 was obtained from Thermo Fisher Scientific (Waltham, MA). The anti–penta-histidine (His) antibody–horseradish peroxidase (HRP) conjugate was obtained from QIAGEN (Hilden, Germany). The anti–human kappa and anti–human lambda antibody–HRP conjugate was obtained from Abcam (Cambridge, UK). 3,3′,5,5′-Tetramethylbenzidine solution was purchased from Dako (Carpinteria, CA). DBCO-PEG4-maleimide and DBCO-PEG4-DBCO were purchased from Click Chemistry Tools (Scottsdale, AZ). Mertansine was obtained from Santa Cruz Biotechnology (Dallas, TX). The reaction buffer was composed of 20 mM sodium citrate (pH 6.0) and 150 mM NaCl. His MultiTrap™ HP plates were purchased from GE Healthcare (Little Chalfont, UK). Recombinant glutathione S-transferase–tagged human epidermal growth factor receptor 2 (HER2-GST) was prepared and validated in house. Recombinant human insulin-like growth factor-1 receptor (IGF1R) was obtained from R&D Systems (Minneapolis, MN). The breast cancer cell line BT-474 was obtained from the American Type Culture Collection (Manassas, VA) and cultured in RPMI1640 medium (Nacalai Tesque, Tokyo) containing 10% fetal bovine serum (FBS; GIBCO, Waltham, MA) and 10 μg/mL bovine insulin (Thermo Fisher Scientific). Recombinant human insulin-like growth factor 1 (IGF1) was obtained from R&D Systems (Minneapolis, MN). Cell Titer-Glo was purchased from Promega (Fitchburg, WI).

3.2 Expression and Purification of Fab Variants

Cixutumumab (Cix) LC variable region (VL) sequence was joined to CLλ (Cλ2: Accession J00253), forming the LC. Expression and purification of Fab variants containing *o*-Az-Z-Lys were performed as previously reported [6]. Briefly, the plasmid for expression of Fab variants incorporated with *o*-Az-Z-Lys, pFLAG-CTS-PylTS-Fab, carrying Fab HCs and LCs and the PylRS gene containing two mutations (Y306A and Y384F), was transformed into the *E. coli* strain W3110 RFzero, an RF-1–knockout *E. coli* W3110 strain established in our previous study. For *o*-Az-Z-Lys–incorporated Fab expression, single colonies of W3110 RFzero transformants were grown overnight at 37°C in 10 mL of Luria-Bertani medium containing 0.1 mg/mL Z-Lys and 100 μg/mL ampicillin. Overnight cultures were diluted with 200 mL of Super Broth containing 1 mM *o*-Az-Z-Lys in place of Z-Lys and incubated at 37°C until OD600 reached 2.0, followed by further incubation at 22°C overnight following the addition of 1 mM isopropyl-β-D-thiogalactopyranoside. Cells were centrifuged at 7,000 rpm for 3 min, and cell pellets were frozen at −80°C. The purification of Fab variants by Protein G affinity chromatography was performed as described previously [18].

3.3 ASA Ratio

The solvent-accessible surface area (ASA ratio [S]) was calculated using the MOE ASA Calculator program (MOLSIS Inc., Tokyo, Japan) operated by the Molecular Operating Environment 2013.08 (Chemical Computing Group, Montreal Inc., Canada) based on the structural information in the Protein Data Bank (PDB) for CR4354, an anti–West Nile Virus monoclonal antibody (PDB ID: 3N9G) as the

representative structure of Fab containing CLλ, assuming that the variants containing *o*-Az-Z-Lys had exactly the same tertiary structure as the PDB entry. To determine the percentage values, the ASA ratio (S) of amino acid "X" in the Gly-X-Gly tripeptide was assumed to be 1.0.

3.4 Copper-Free Click-Chemistry Reaction

A copper-free click-chemistry reaction between *o*-Az-Z-Lys in the Fab and DIBO-Alexa Fluor 488 was performed previously [6]. Briefly, 5 μM of Fab reacted with 200 μM of DIBO-Alexa Fluor 488 overnight at room temperature. Reaction efficiency was determined by separating the conjugates by cation-exchange chromatography on a TSKgel SP-5PW column (Tosoh, Tokyo, Japan) using the Prominence HPLC system (Shimadzu, Kyoto, Japan) with buffer A (20 mM acetate buffer [pH 5.0]) as the initial buffer. Separation was performed at a flow rate of 1 mL/min at 25°C using a gradient of buffer B (20 mM acetate buffer [pH 5.0] and 1 M NaCl) from 0% to 100% in the mixture of buffer A and buffer B for 20 min. The proportion of the protein moiety of the conjugate was calculated based on absorbance at 280 nm, whereas that of the Alexa Fluor 488 moiety was calculated based on absorbance at 495 nm. Reaction efficiency was determined by calculating the molar ratio between these moieties and considering that their Fabs contained one and two *o*-Az-Z-Lys sites, respectively.

3.5 Binding Analysis by ELISA

The 96-well enzyme-linked immunosorbent assay (ELISA) plate was coated with human IGF1R or HER2-GST fusion protein (1 μg/mL) and incubated overnight at

4°C. After washing with Tris-buffered saline containing 0.05% Tween-20 (TBST), 150 µL of 1% bovine serum albumin in phosphate-buffered saline (PBS) was added to each well and incubated for 1 h at room temperature. Samples were prepared in 1% bovine serum albumin in PBS at a range of concentrations, added (50 µL) to each well, and then incubated for 1 h at room temperature. The wells were then washed with TBST, followed by incubation with 50 µL of 1,000 times diluted anti–penta-His antibody–HRP conjugate, anti–human kappa–HRP conjugate, or anti–human lambda–HRP conjugate for 1 h at room temperature. The wells were washed again with TBST and developed using 50 µL of 3,3′,5,5′-tetramethylbenzidine.

3.6 Analytical Methods

o-Az-Z-Lys–incorporated Fabs and Fab-dimers were all analyzed by sodium dodecyl sulfate polyacrylamide gel electrophoresis (SDS-PAGE) and Coomassie staining. Liquid chromatography–mass spectrometry (LC-MS) analysis and differential-scanning calorimetry were performed as described previously [6].

3.7 Preparation of Cix-Fab–DM1 Conjugates

o-Az-Z-Lys–incorporated Cix-Fab molecules obtained after Protein G purification were further purified on a cation-exchange column (Mono S 5/50 GL; GE Healthcare) using AKTA fast protein liquid chromatography (GE Healthcare) with mobile phase A (20 mM sodium citrate [pH 6.0]) and mobile phase B (1 M NaCl and 20 mM sodium citrate [pH 6.0]). A linear gradient of 0% to 100% mobile phase B was used to remove endotoxin from the samples. The buffer exchange to reaction buffer was performed using an Amicon Ultra-0.5 device (Merck Millipore, Billerica,

MA). *o*-Az-Z-Lys–incorporated Cix-Fab molecules were then conjugated with an eight-fold molar excess of DBCO-PEG4-maleimide linker in the reaction buffer overnight at 4°C. Removal of the free DBCO-PEG4-maleimide and buffer exchange to reaction buffer were conducted using an Amicon Ultra-0.5 device (Merck Millipore). DBCO-PEG4-maleimide–conjugated Fab molecules were conjugated with a 10-fold molar excess of thiol-containing DM1, a cytotoxin. Prior to *in vitro* cytotoxicity assays, unconjugated toxins were removed using an Amicon Ultra-0.5 device, and formation of the Cix-Fab–DM1 conjugate was confirmed by LC-MS analysis as described above.

3.8 Preparation of Cix-Fab×Tra-Fab Bispecific Dimers

The *o*-Az-Z-Lys–incorporated Cix-Fabs after Protein G purification were conjugated with a 20-fold molar excess of the DBCO-PEG4-DBCO linker in the reaction buffer overnight at room temperature. Removal of the free DBCO-PEG4-DBCO and buffer exchange to reaction buffer were conducted using the Amicon Ultra-0.5 device (Merck Millipore). DBCO-PEG4-DBCO–conjugated Cix-Fabs were applied (50 μg/well) into His MultiTrap™ HP plates (GE Healthcare) and incubated for 10 min at room temperature for the Fab molecules to be captured by the hexa-His tag. Following centrifugation, 50 μg/well of *o*-Az-Z-Lys–incorporated trastuzumab (Tra)-Fab molecule was added, followed by incubation overnight at room temperature to generate Cix-Fab×Tra-Fab bispecific dimers. The generated Cix-Fab×Tra-Fab bispecific dimers were eluted with 500 mM imidazole in Dulbecco PBS (pH 7.4) and separated from unreacted Tra-Fab monomer by size-exclusion chromatography using Superdex 200 increase column (GE Healthcare) and AKTA

FPLC (GE Healthcare).

3.9 *In vitro* Cytotoxicity Assays for MCF-7

MCF-7 cells maintained in RPMI1640 supplemented with 10% FBS were centrifuged and seeded onto 96-well plates (5,000 cells per well) in culture medium and treated the following day with a series of diluted Cix-Fab–DM1 conjugates. Cells were incubated for 5 days at 37°C in a humidified atmosphere of 5% CO_2. Cell Titer-Glo luminescent cell viability (Promega) reagent was added to the wells, incubated at room temperature for 10 min, and the luminescent signal was measured using the ARVO X3 system (PerkinElmer). The results are expressed as a percentage of growth compared to the control group.

3.10 Cell-Proliferation Assays for BT-474

BT-474 cells maintained in RPMI1640 supplemented with 10% FBS and 10 μg/mL bovine insulin were centrifuged and seeded onto 96-well plates (10,000 cells per well) in culture medium added with 2% FBS and 3 nmol/L human IGF-1 and treated the following day with a series of diluted Tra-Fab, Cix-Fab, and Tra-Fab×Cix-Fab bispecific dimers. Cells were incubated for 5 days at 37°C in a humidified atmosphere of 5% CO_2. Cell Titer-Glo luminescent cell viability reagent (Promega) was added to the wells, incubated at room temperature for 10 min, the luminescent signal was measured, and the results expressed as a percentage of growth compared to the control group as described above.

4 Results

4.1 Selection Strategy for Chemical Conjugation Using *o*-Az-Z-Lys in CLλ

In this study, we used cixutumumab, a human IgG1 anti-IGF1R antibody that has CLλ [7], as a model antibody for selecting the positions for chemical conjugation using *o*-Az-Z-Lys. The degree of solvent exposure in a position as represented by the ASA affects the efficiency of chemical conjugation. In several studies using *p*-AzF, which has a relatively short side chain, conjugation sites were selected among positions with ASA values ≥0.4 for efficient conjugation in antibody molecules. However, in our prior study using *o*-A-Z-Lys, which contains the reaction groups at the end of a long side chain (Figure 3), we found that positions with a moderate ASA range (0.2 to 0.4) in CH1 and CLκ are suitable for efficient *o*-Az-Z-Lys conjugation [6]. Then, we attempted to expand the survey to CLλ. To this end, we selected 20 positions exhibiting ASA values between 0.2 and 0.4 in CLλ Fab (Figure 7).

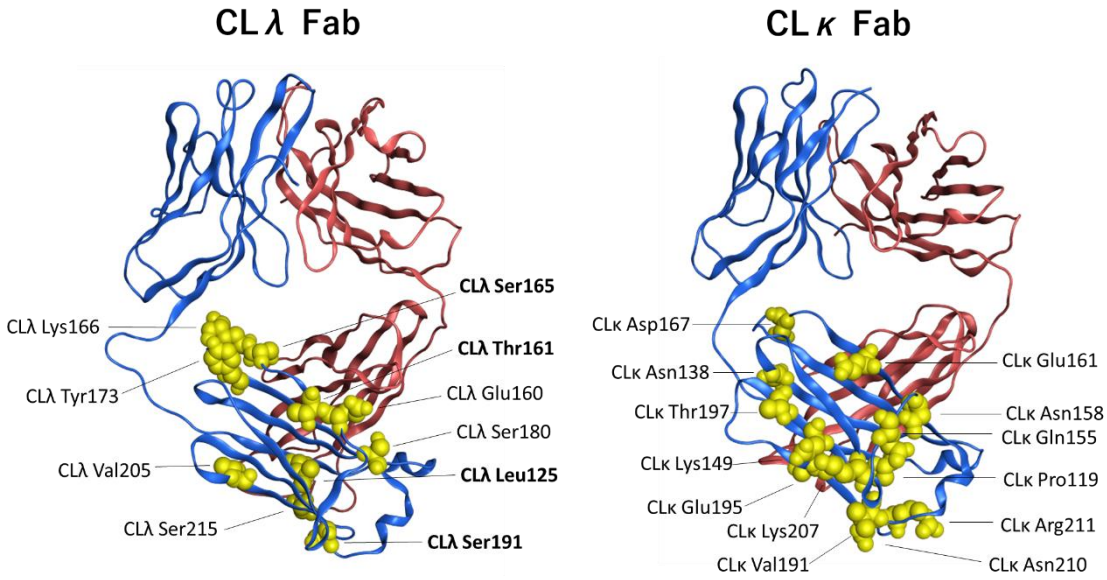

Figure 7. Locations of the selected positions in the tertiary structure of a representative CLλ Fab and CL *κ* Fab

Highly reactive positions are mapped in the crystal structures of human Fab fragments of the λ (left panel, PDB ID: 3N9G) and κ (right panel, PDB ID: 1N8Z) isotypes. The heavy and light chains are represented by red and blue ribbons, respectively. The residues to be replaced with o-Az-Z-Lys are represented in the CPK model. The CLλ positions involved in the formation of Cix×Tra Fab-dimers are indicated with bold letters.

CLλ, λ light chain constant region; CPK, Corey-Pauling-Koltun; Fab, antigen-binding fragment; *o*-Az-Z-Lys, *Nε*-(*o*-Azidobenzyloxycarbonyl)-L-lysine; PDB, Protein Data Bank; SPAAC, strain-promoted alkyne-azide cycloaddition.

4.2 Identification of Multiple Positions Useful for Chemical Conjugation in the Fab CLλ

The selected 20 positions exhibiting ASA ratio values between 0.2 and 0.4 in the Cix-Fab CLλ were examined using RF-1–knockout *E. coli* W3110 cells. The yields of the Cix-Fab variants containing *o*-Az-Z-Lys were comparable to those of wild-type Cix-Fab (0.1 mg/100 mL culture) except for four variants (CLλ 151, 171, 210, and 213); these variants showed significantly lower yields. Assembly of the HCs and LCs was confirmed by nonreducing SDS-PAGE (Figure 8). MS analyses confirmed that the changes in masses were consistent with those expected for the replacements of the amino acid at the UAG codon by *o*-Az-Z-Lys (Figure 8). Signals indicating contamination by other amino acids at the UAG positions were not observed. ELISA showed that the incorporation of *o*-Az-Z-Lys at any site did not impair the antigen-binding activity of Cix-Fab (Figure 8).

A)

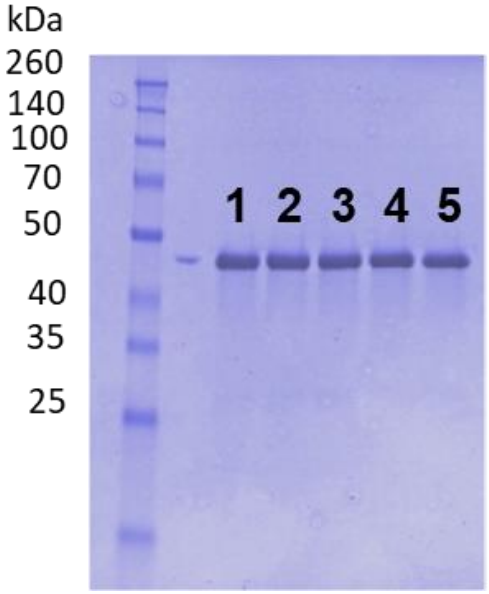
kDa
260
140
100
70
50
40
35
25
1 2 3 4 5

B)

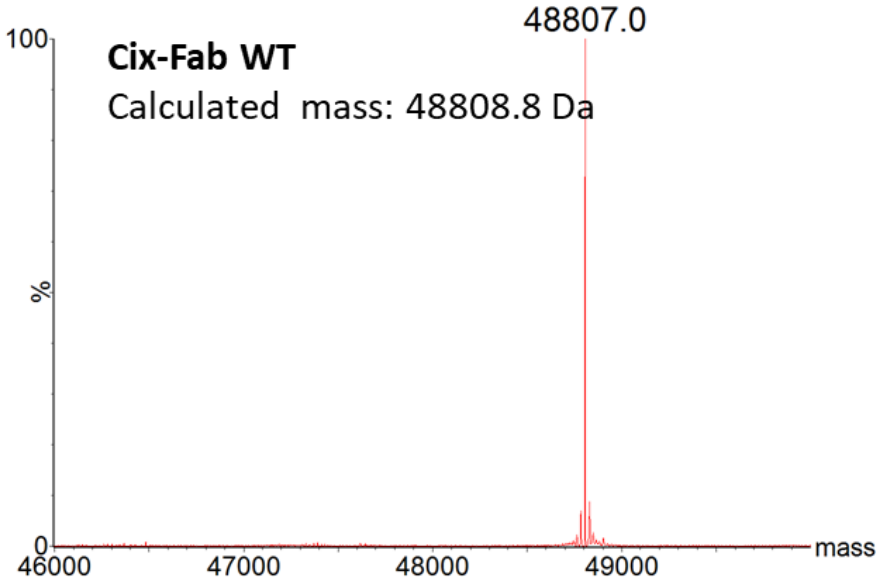
48807.0
Cix-Fab WT
Calculated mass: 48808.8 Da
100
%
0
46000
47000
48000
49000
mass

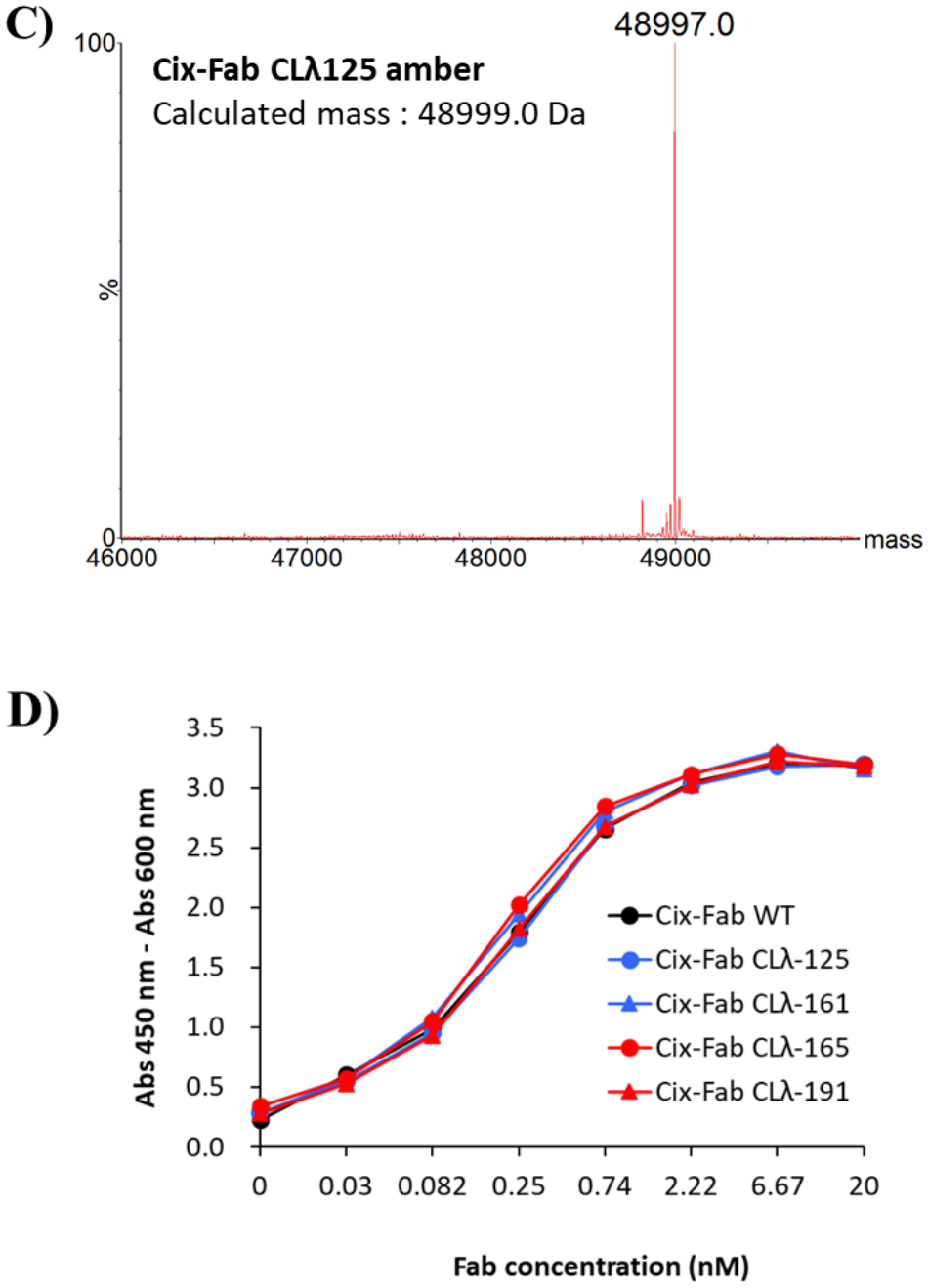

Figure 8. Quality checks of the synthesized Cix-Fab variants. Representative data

are shown.

(A) Nonreducing SDS-PAGE analyses of the WT Cix-Fab (lane 1) and the variants containing *o*-Az-Z-Lys at the positions CLλ-125, CLλ-161, CLλ-165, and CLλ-191 (lanes 2 to 5, respectively).

(B, C) MS analyses of the WT Cix-Fab and the variant containing *o*-Az-Z-Lys at the CLλ-125 position.

(D) ELISA results for Cix-Fab variants containing *o*-Az-Z-Lys at the indicated positions. Increasing amounts of Fab were added to immobilized IGF1R and detected with anti–His-tag HRP and 3,3′,5,5′-tetramethylbenzidine substrate.

Cix, cixutumumab; CLλ, λ light chain constant region; ELISA, enzyme-linked immunosorbent assay; Fab, antigen-binding fragment; His, histidine; HRP, horseradish peroxidase; IGF1R, insulin-like growth factor-1 receptor; MS, mass spectrometry; *o*-Az-Z-Lys, *Nε*-(*o*-Azidobenzyloxycarbonyl)-L-lysine; SDS-PAGE, sodium dodecyl sulfate polyacrylamide gel electrophoresis; WT, wild-type.

We then examined *o*-Az-Z-Lys reactivity in these variants during SPAAC using the DIBO-Alexa Fluor 488 dye as a model payload. Wild-type Cix-Fab showed no reactivity, whereas most of the variants were efficiently labeled and exhibited reactivities ranging from 80% to 90% (Figure 9 and Table 1). Furthermore, 10 of the 16 Cix-Fab variants were examined for thermal stability by differential-scanning calorimetry. The melting temperature (T_m) of the wild-type Cix-Fab was determined as 78.1°C, and most of the examined variants, except for CLλ-173, showed similar

stabilities. These results indicated that the incorporation of *o*-Az-Z-Lys at invariant positions had little effect on the structural stability of Fab molecules (Table 1).

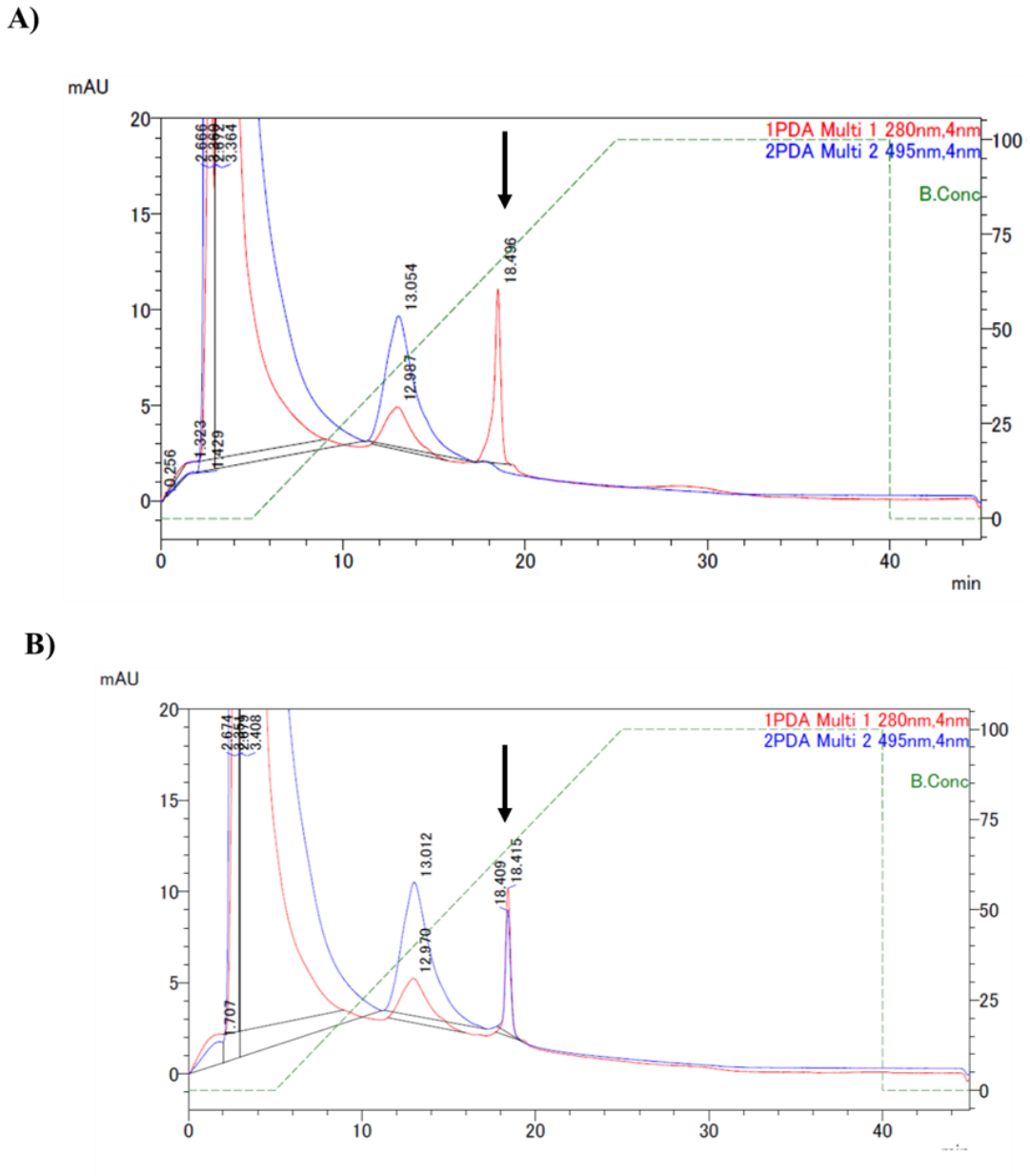

Figure 9. Quantification of SPAAC using the DIBO-Alexa Fluor 488 dye as a model payload.

Reaction efficiency was determined by separating the conjugates by cation-exchange

chromatography on the HPLC system. Separation was performed by NaCl gradient. The proportion of the protein moiety of the conjugates (arrows) was calculated based on absorbance at 280 nm, whereas that of the Alexa Fluor 488 moiety was calculated based on absorbance at 495 nm.

(A) Wild-type Cix-Fab showed no reactivity.

(B) Absorbance at 495 nm was observed for Cix-Fab variants containing *o*-Az-Z-Lys. The typical result of Cix-Fab variants containing *o*-Az-Z-Lys at CLλ-165 position is shown as the representative.

Cix, cixutumumab; CLλ, λ light chain constant region; Fab, antigen-binding fragment; HPLC, high-performance liquid chromatography; *o*-Az-Z-Lys, *N*ε-(*o*-Azidobenzyloxycarbonyl)-L-lysine; SPAAC, strain-promoted alkyne-azide cycloaddition.

Table 1. ASA ratios of the indicated positions in CLλ and the T_m values and SPAAC reactivities of Cix-Fab variants containing *o*-Az-Z-Lys at these positions.

Positions (EU number)	Residue	ASA ratio (S)	SPAAC reactivity (%)	T_m (°C)
WT	-	-	0.0	78.1
119	Pro	0.24	80.5	N/A
125	Leu	0.28	116.0	80.2
137	Ser	0.28	32.0	N/A
149	Lys	0.22	75.4	N/A
151	Asp	0.21	N/A	N/A
160	Glu	0.24	92.8	77.9
161	Thr	0.24	90.5	77.4
165	Ser	0.29	92.9	77.0
166	Lys	0.17	94.1	75.8
171	Asn	0.40	N/A	N/A
173	Tyr	0.24	90.8	74.0
180	Ser	0.38	91.9	77.8
189	His	0.35	83.4	N/A
191	Ser	0.29	99.8	77.8
195	Gln	0.24	88.5	77.5
197	Thr	0.40	77.4	N/A
205	Val	0.34	93.6	77.0
210	Ala	0.33	N/A	N/A
213	Glu	0.35	N/A	N/A
215	Ser	0.36	108.6	N/A

All of the indicated reactivities, calculated as described in Materials and Methods, represent the mean of two experiments.

ASA, solvent-accessible surface area; Cix, cixutumumab; CLλ, λ light chain constant region; Fab, antigen-binding fragment; N/A, not available; *o*-Az-Z-Lys, *Nε*-(*o*-Azidobenzyloxycarbonyl)-L-lysine; SPAAC, strain-promoted alkyne-azide cycloaddition; T_m, melting temperature; WT, wild-type.

4.3 Preparation of Cix-Fab–Mertansine DM1 Conjugates

ADCs have made significant progress in the oncology field, as illustrated by the two United States FDA–approved drugs ado-trastuzumab emtansine (KADCYLA) and brentuximab vedotin (ADCETRIS) and ongoing clinical studies [41]. As an ideal delivery platform, ADCs are showing great potential for nononcological indications such as immune modulation and anti-infection [42]. Site-specific conjugation technology enables the production of homogeneous materials and improvement of pharmacokinetic profiles and has been advanced by utilizing unpaired cysteines, enzymatic modifications, and nnAAs [43-45]. The major advantage of using nnAAs is that it enables the application of bio-orthogonal-conjugation chemistry, such as alkyne-azide cycloaddition and click chemistry [16, 22]. In this study, we selected four positions (CLλ 125, 161, 165, and 191) as highly reactive positions, and to demonstrate the feasibility of site-specific ADCs using our approach, four variants containing *o*-Az-Z-Lys residues at defined sites were each conjugated with DM1 via a DBCO-PEG4-maleimide linker (Figure 10). The formation of the Cix-Fab–DM1 conjugates was confirmed by LC-MS analysis (Figure 11 and Table 2). SDS-PAGE and ELISA analyses showed that DM1 conjugation at any site did not impair the assembly of HCs and LCs and antigen-binding activity (Figure 12 and Figure 13).

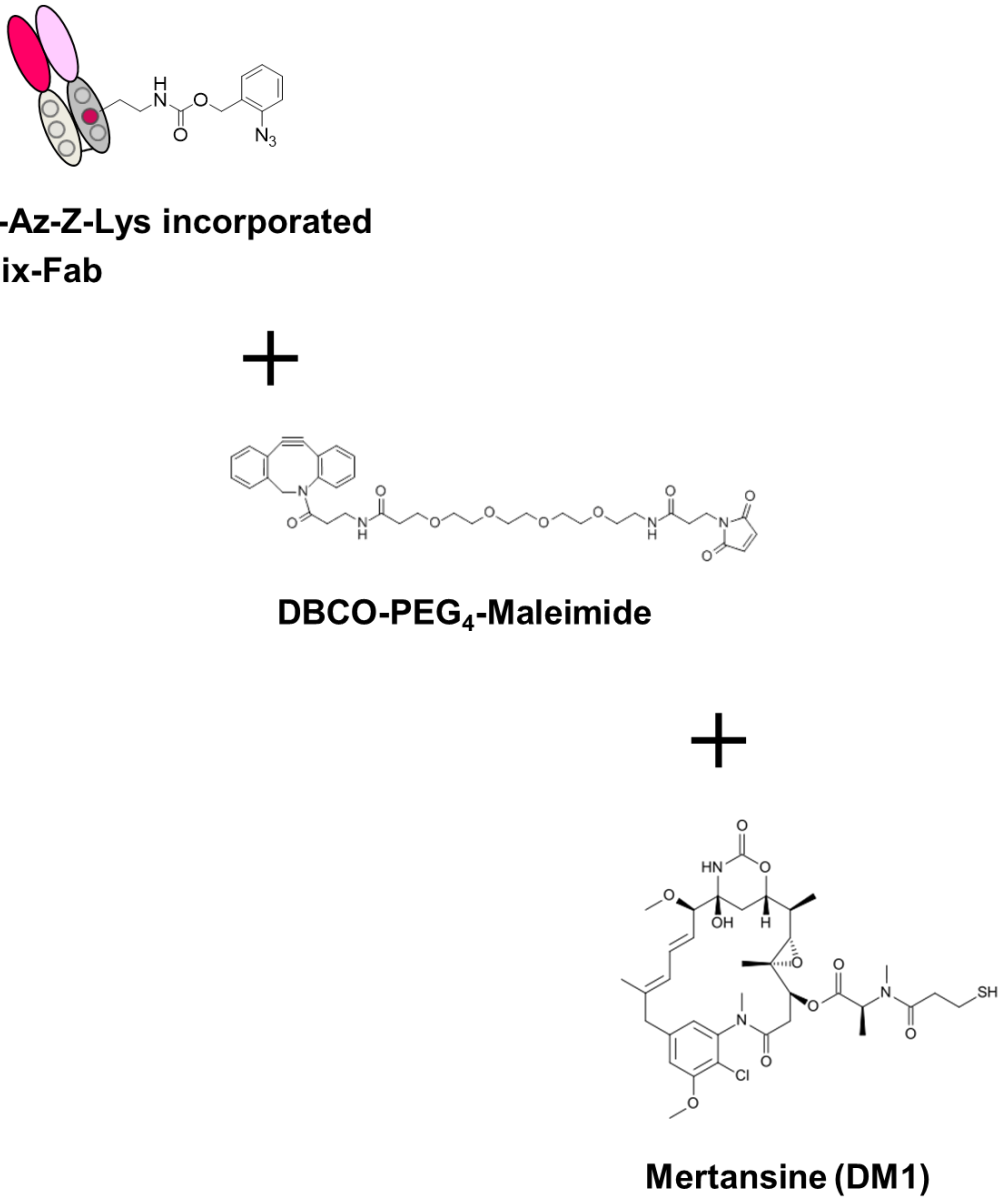

Figure 10. The schematic of preparation of Cix-Fab–DM1 conjugates.

The Cix-Fab–DM1 conjugates were prepared sequentially. *o*-Az-Z-Lys–incorporated Cix-Fab variants were separated from endotoxin using cation-exchange chromatography, conjugated with DBCO-PEG4-maleimide linker, and purified. They were then conjugated with thiol-containing DM1.

Cix, cixutumumab; DBCO, dibenzylcyclooctyne; Fab, antigen-binding fragment; *o*-Az-Z-Lys, *Nε*-(*o*-Azidobenzyloxycarbonyl)-L-lysine; PEG, polyethylene glycol.

A)

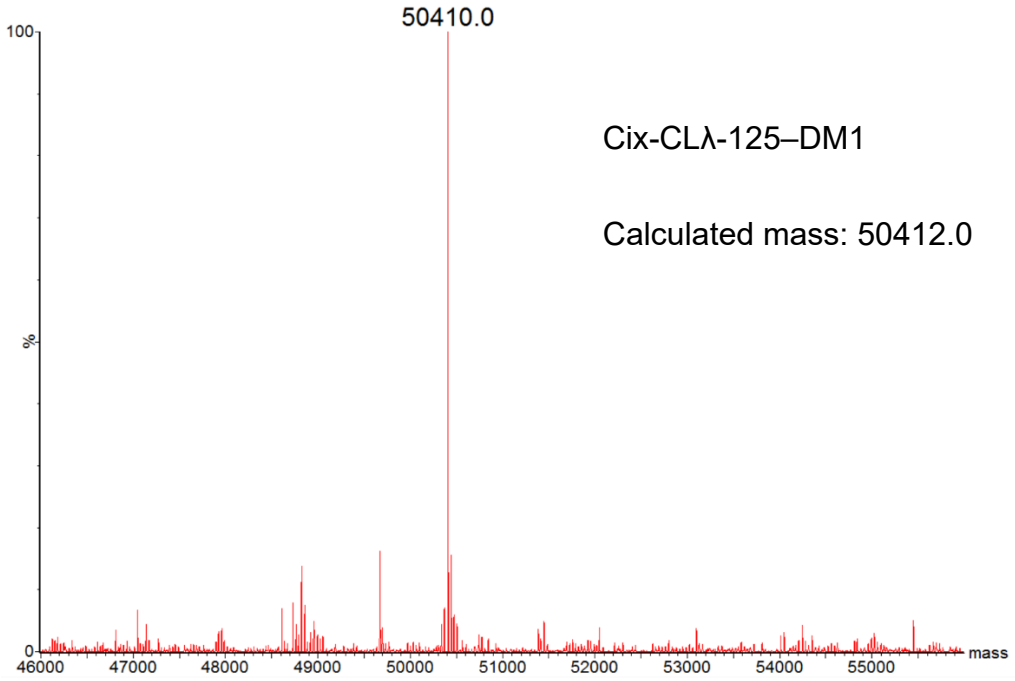
50410.0
100
%
0
46000
47000
48000
49000
50000
51000
52000
53000
54000
55000
mass
Cix-CLλ-125–DM1
Calculated mass: 50412.0

B)

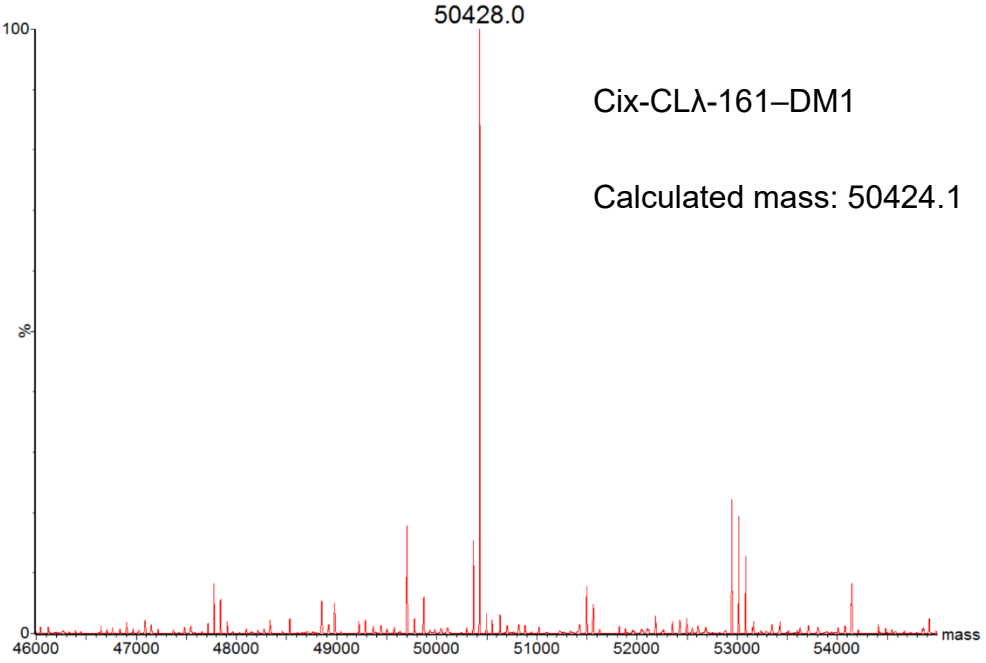
50428.0
100
%
0
46000
47000
48000
49000
50000
51000
52000
53000
54000
mass
Cix-CLλ-161–DM1
Calculated mass: 50424.1

C)

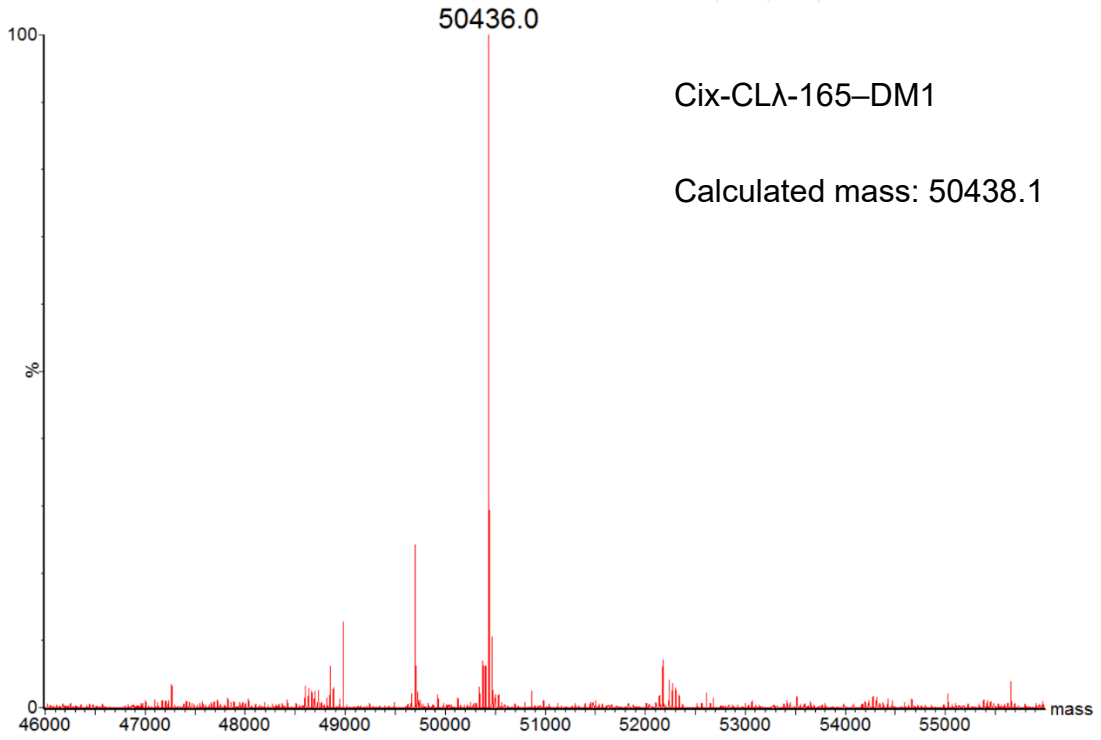
50436.0
100
%
0
46000
47000
48000
49000
50000
51000
52000
53000
54000
55000
mass
Cix-CLλ-165–DM1
Calculated mass: 50438.1

D)

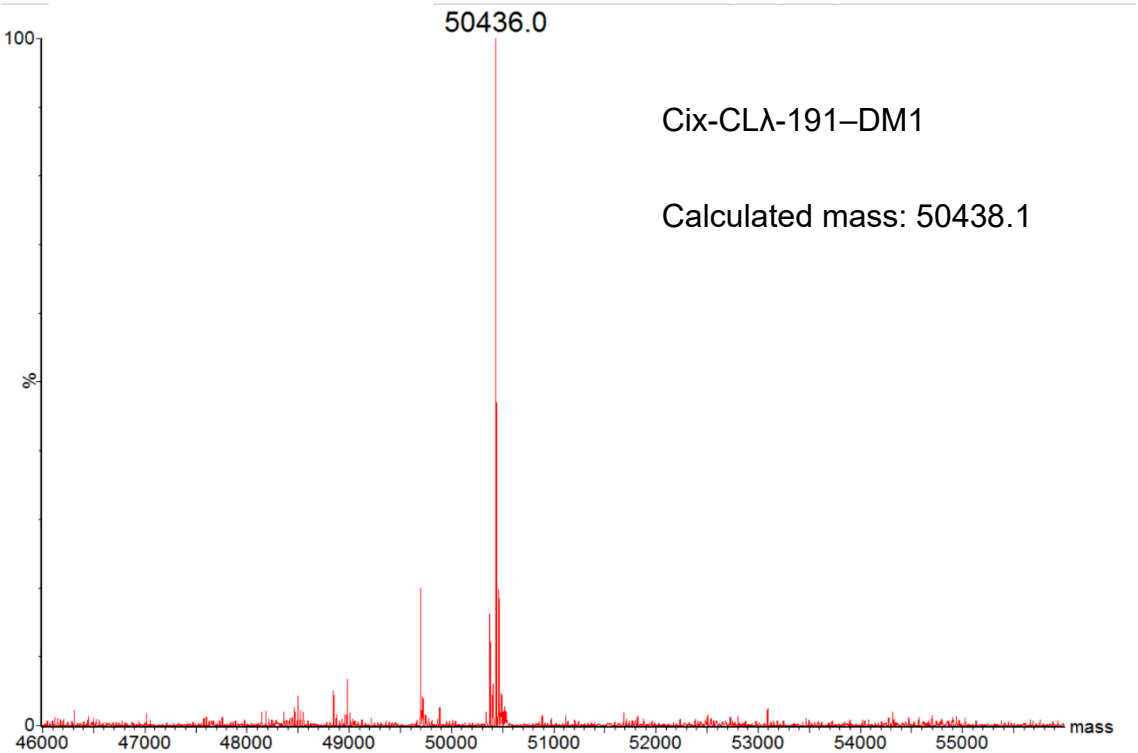
50436.0
100
%
0
46000
47000
48000
49000
50000
51000
52000
53000
54000
55000
mass
Cix-CLλ-191–DM1
Calculated mass: 50438.1

Figure 11. MS analysis of Cix-Fab–DM1 conjugate.

The results for the Cix-Fab–DM1 conjugate using variants containing *o*-Az-Z-Lys at the positions CLλ-125, CLλ-161, CLλ-165, and CLλ-191 (A to D, respectively).

Cix, cixutumumab; CLλ, λ light chain constant region; Fab, antigen-binding fragment; MS, mass spectrometry; *o*-Az-Z-Lys, *Nε*-(*o*-Azidobenzyloxycarbonyl)-L-lysine.

Table 2. MS analyses of Cix-Fab–DM1 conjugates.

Fab-dimer	Calculated mass (Da)	Observed mass (Da)
Cix-CLλ-125–DM1	50412.0	50410.0
Cix-CLλ-161–DM1	50424.1	50428.0
Cix-CLλ-165–DM1	50438.1	50436.0
Cix-CLλ-191–DM1	50438.1	50436.0

Cix, cixutumumab; CLλ, λ light chain constant region; Fab, antigen-binding fragment; MS, mass spectrometry.

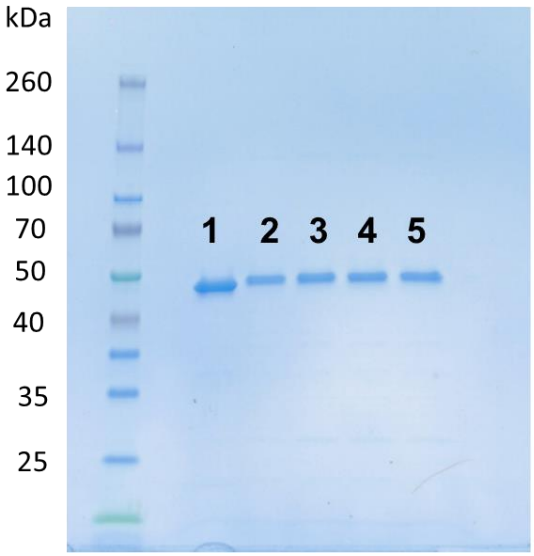

Figure 12. Quality checks of the synthesized Cix-Fab–DM1 conjugates.

Nonreducing SDS-PAGE analyses of the wild-type Cix-Fab (lane 1) and Cix-Fab–DM1 conjugates composed of the variants containing *o*-Az-Z-Lys at the positions CLλ-125, CLλ-161, CLλ-165, and CLλ-191 (lanes 2 to 5, respectively).

Cix, cixutumumab; CLλ, λ light chain constant region; Fab, antigen-binding fragment; *o*-Az-Z-Lys, *Nε*-(*o*-Azidobenzyloxycarbonyl)-L-lysine; SDS-PAGE, sodium dodecyl sulfate polyacrylamide gel electrophoresis.

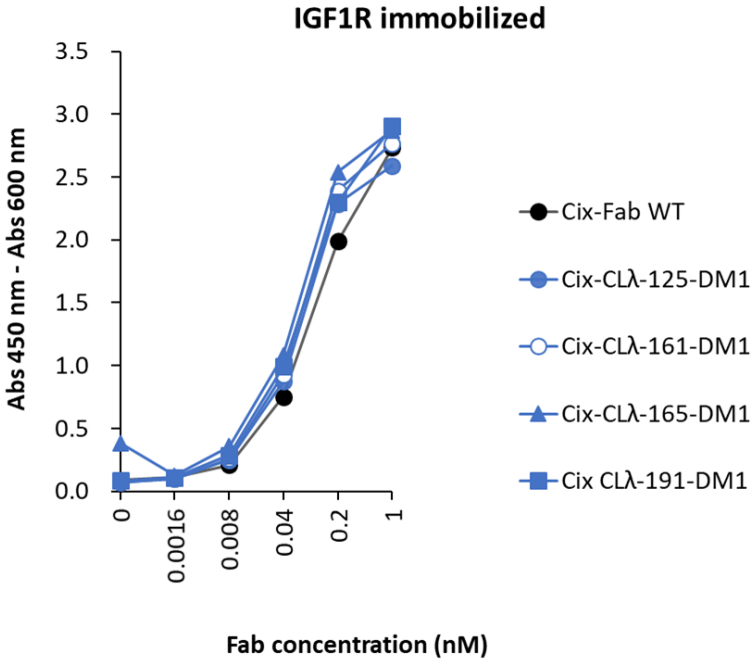

Figure 13. ELISA analysis of antigen-binding activity of Cix-Fab–DM1 conjugates.

The result of Cix-Fab–DM1 conjugates using variants containing *o*-Az-Z-Lys at four positions.

Cix, cixutumumab; CLλ, λ light chain constant region; ELISA, enzyme-linked immunosorbent assay; Fab, antigen-binding fragment; IGF1R, insulin-like growth factor-1 receptor; WT, wild-type.

4.4 *In vitro* Cytotoxicity of Cix-Fab–Mertansine DM1 Conjugates

We analyzed *in vitro* cytotoxicity of Cix-Fab–DM1 conjugates using MCF-7 cells, an IGF1R-overexpressing cell line [46]. It has been reported that Cix-IgG induces IGF1R dimerization leading to surface receptor internalization and degradation [47]. However, a study using anti-IGF1R×anti–epidermal growth factor receptor (EGFR) bispecific antibodies showed that the monomeric anti-IGF1R binding arm shows significantly reduced internalization and degradation of cell surface IGF1R because of the absence of IGF1R dimerization [48].

Cix-Fab–DM1 conjugates showed no cytotoxicity when applied alone but showed significant cytotoxicity when applied with a monoclonal anti–human lambda antibody as a cross-linker of Cix-Fab–DM1 conjugates to induce IGF1R dimerization and internalization (Figure 14). All four variants showed similar cytotoxicity against MCF-7 cells (Figure 14).

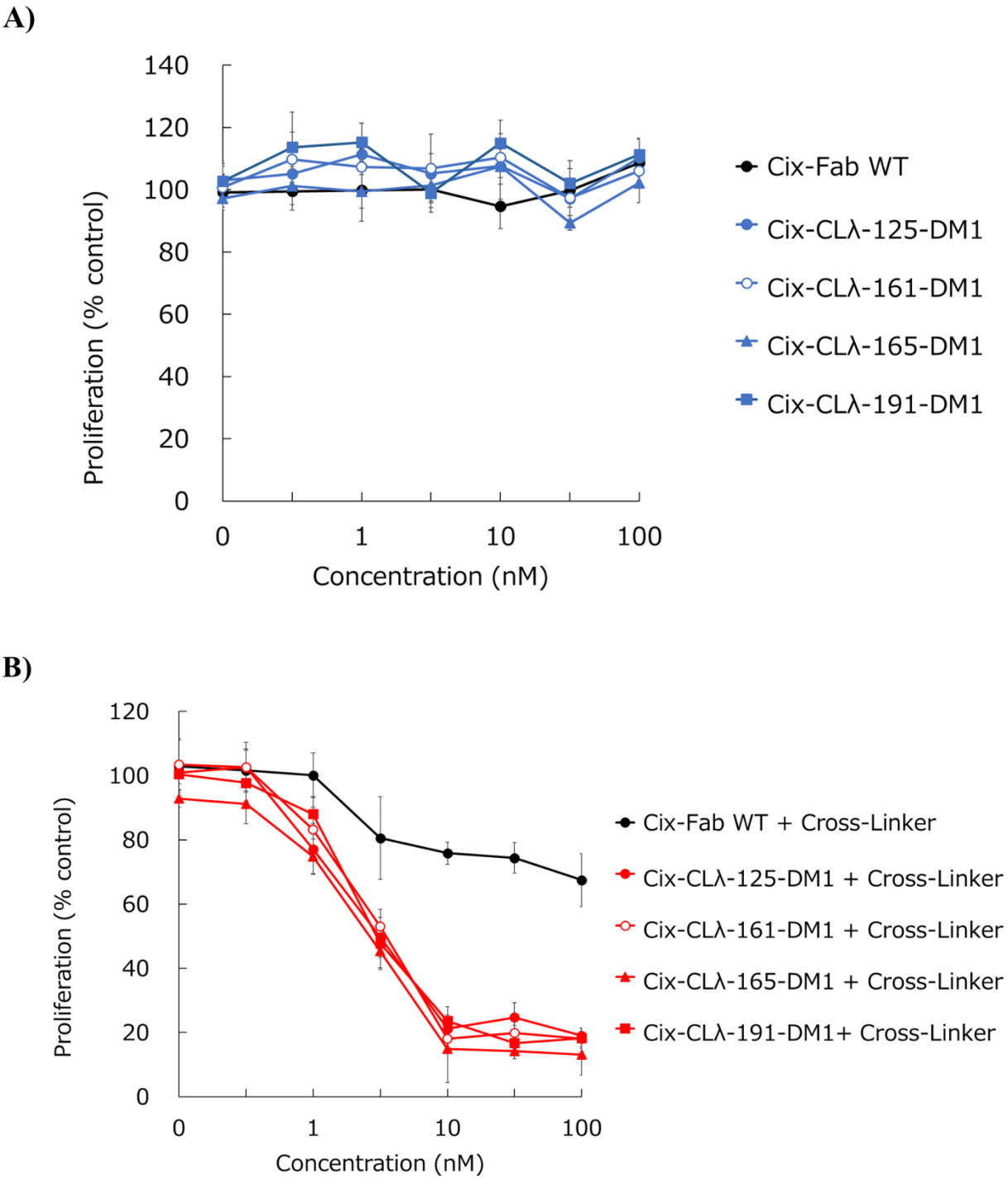

Figure 14. *In vitro* cytotoxicity of Cix-Fab–DM1 conjugates in the IGF1R-overexpressing cell line MCF-7.

(A) No antiproliferative effect was observed without cross-linker.

(B) Potent cytotoxicity was observed with anti–human λ light chain antibody as the cross-linker.

Cix, cixutumumab; CLλ, λ light chain constant region; Fab, antigen-binding fragment; IGF1R, insulin-like growth factor-1 receptor; WT, wild-type.

4.5 Preparation of anti-HER2×anti-IGF1R Bispecific Fab-Dimers

Site-specific conjugation of antibodies through incorporation of nnAAs and bio-orthogonal chemical reaction is a promising strategy to generate the next-generation ADCs [17, 18, 21, 22]. Beyond ADCs, the use of nnAAs is expanding as a useful and feasible method to prepare a wide variety of antibody-based therapeutic molecules including bispecific antibodies [19, 20]. Dual-targeting strategies using bispecific antibodies (simultaneously blocking two cell surface receptors that play an essential role in tumor cell growth, such as the EGFR family, i.e., EGFR, HER2, HER3, and HER4 and the IGF1R) are widely applied in cancer therapy [49]. Recently, Chen et al prepared an anti-HER2×anti-IGF1R bispecific antibody using the knobs-into-holes strategy and reported that their bispecific antibody more effectively inhibited cancer cell proliferation than the parental monoclonal antibodies [50]. We aimed to show that the anti-HER2×anti-IGF1R bispecific Fab-dimers could be constructed from anti-HER2 Tra-Fab and Cix-Fab using chemical conjugation to bind both antigens and exhibit some cytotoxic activity.

In our previous study, we developed a method for one-pot preparation of Fab-dimers, where a Fab containing *o*-Az-Z-Lys was conjugated to another Fab containing *o*-Az-Z-Lys via a chemical linker. Using this method, the selected four variants (CLλ 125, 161, 165, and 191) were used to prepare bispecific Fab-dimers consisting of Tra-Fab and Cix-Fab. Therefore, four Cix-Fab molecules, each containing *o*-Az-Z-Lys at CLλ 125, 161, 165, or 191 positions, were conjugated with the DBCO-PEG4-DBCO linker by SPAAC and then conjugated with Tra-Fab containing *o*-Az-Z-Lys at CLκ 155 or CH1 199, confirmed highly reactive in our previous study. In all eight combinations, we confirmed dimerization by nonreducing SDS-PAGE (Figure 15)

and heterodimerization of Fab molecules by MS analysis (Figure 15, Figure 16, and Table 3). No signal indicating homodimerization was observed. ELISA assay showed that the antigen-binding activity to each antigen (HER2 or IGF1R) was not disturbed by dimerization (Figure 17). These results indicate that the selected positions in CLλ could be used to prepare Fab-based conjugates, such as bispecific Fab-dimers.

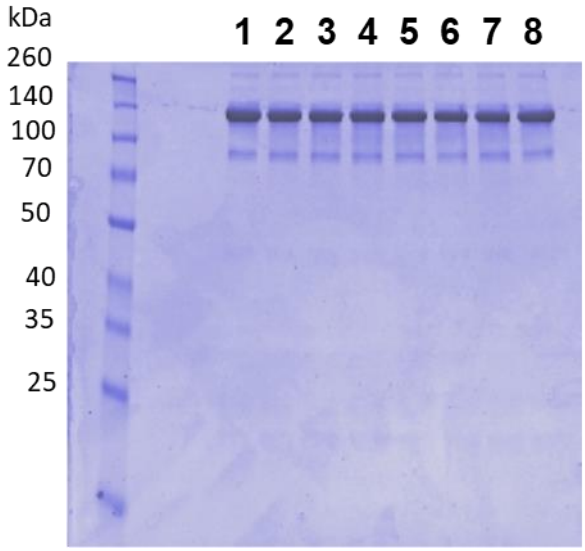

Figure 15. Quality checks of the prepared Cix×Tra bispecific Fab-dimers.

Nonreducing SDS-PAGE analyses of eight combinations of the Fab-dimers. CLλ-125, CLλ-161, CLλ-165, and CLλ-191 combined with Tra-Fab CLκ-155 (lanes 1 to 4, respectively) and CLλ-125, CLλ-161, CLλ-165, and CLλ-191 combined with Tra-Fab CH1-199 (lanes 5 to 8, respectively).

CH1, first constant region of the heavy chain; Cix, cixutumumab; CLκ, κ light chain constant region; CLλ, λ light chain constant region; Fab, antigen-binding fragment; SDS-PAGE, sodium dodecyl sulfate polyacrylamide gel electrophoresis; Tra, trastuzumab.

A)

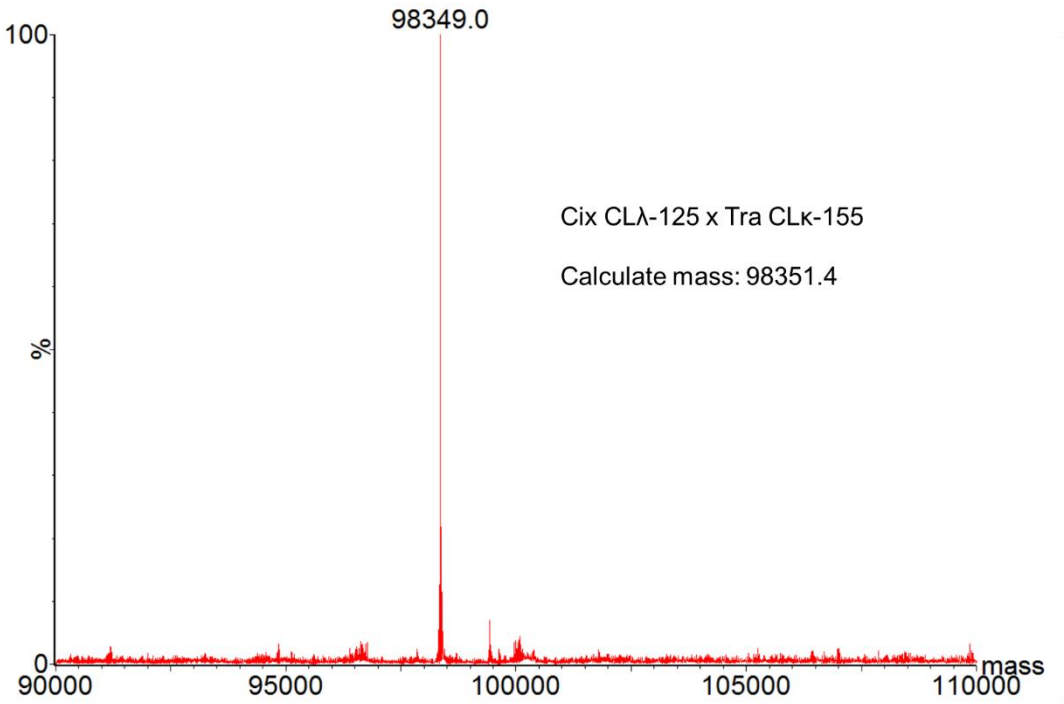
98349.0
100
%
0
Cix CLλ-125 x Tra CLκ-155
Calculate mass: 98351.4
90000
95000
100000
105000
110000
mass

B)

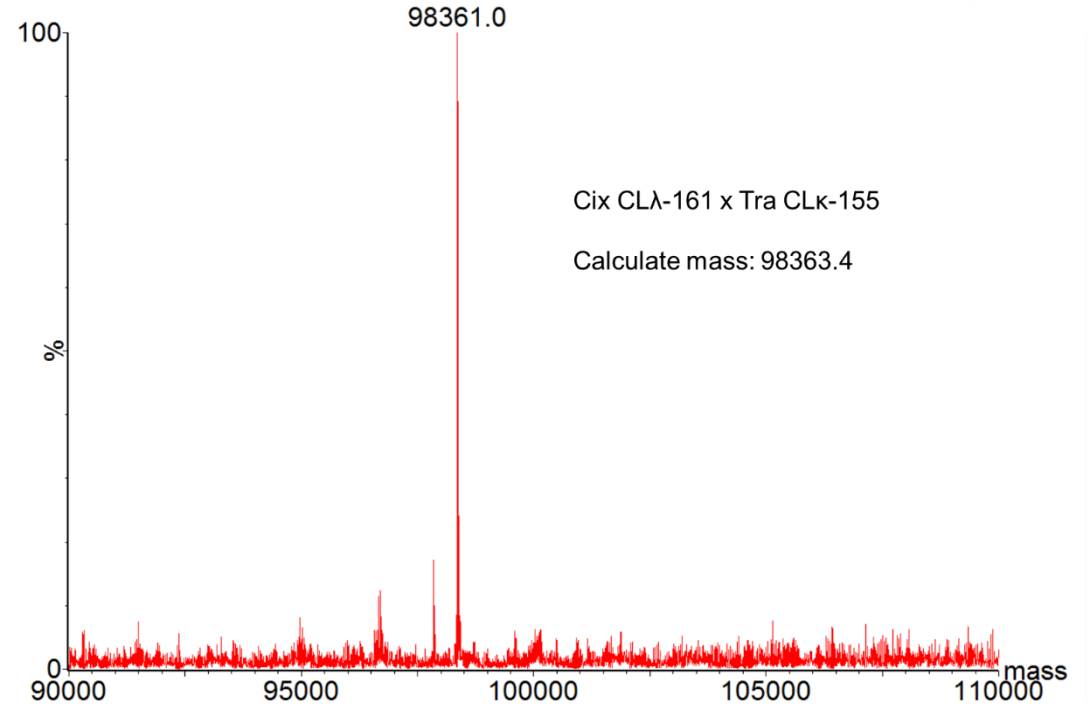
98361.0
100
%
0
Cix CLλ-161 x Tra CLκ-155
Calculate mass: 98363.4
90000
95000
100000
105000
110000
mass

C)

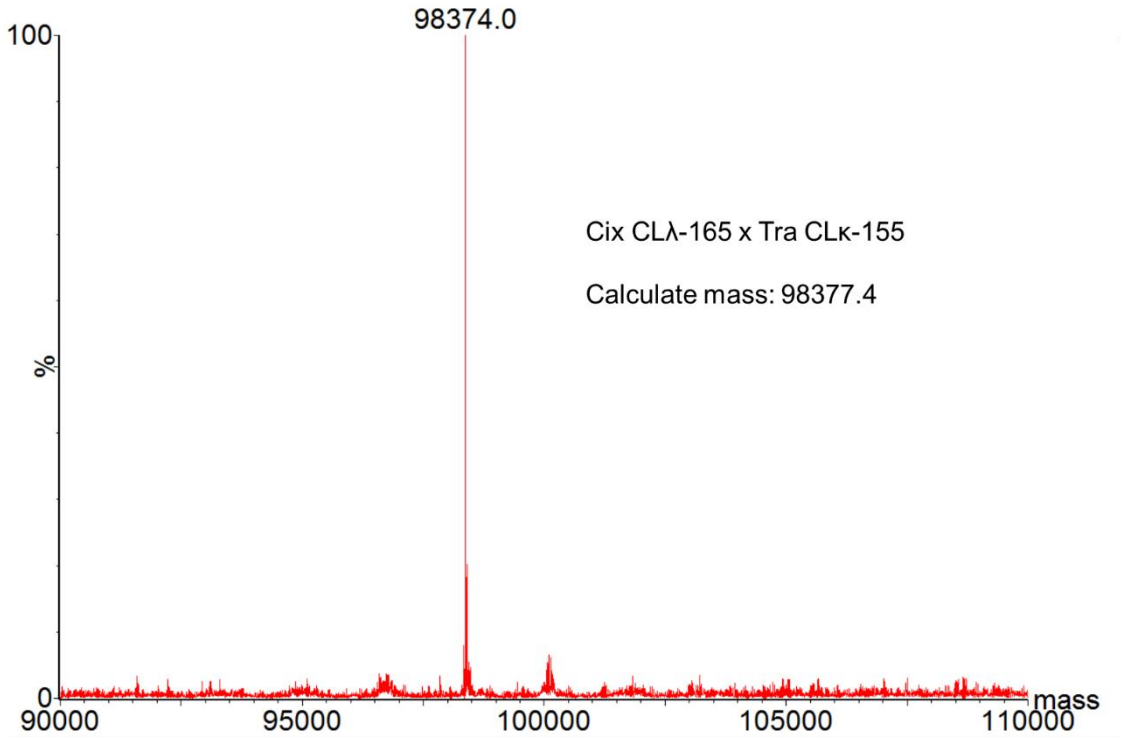
98374.0
100
%
0
Cix CLλ-165 x Tra CLκ-155
Calculate mass: 98377.4
90000
95000
100000
105000
110000
mass

D)

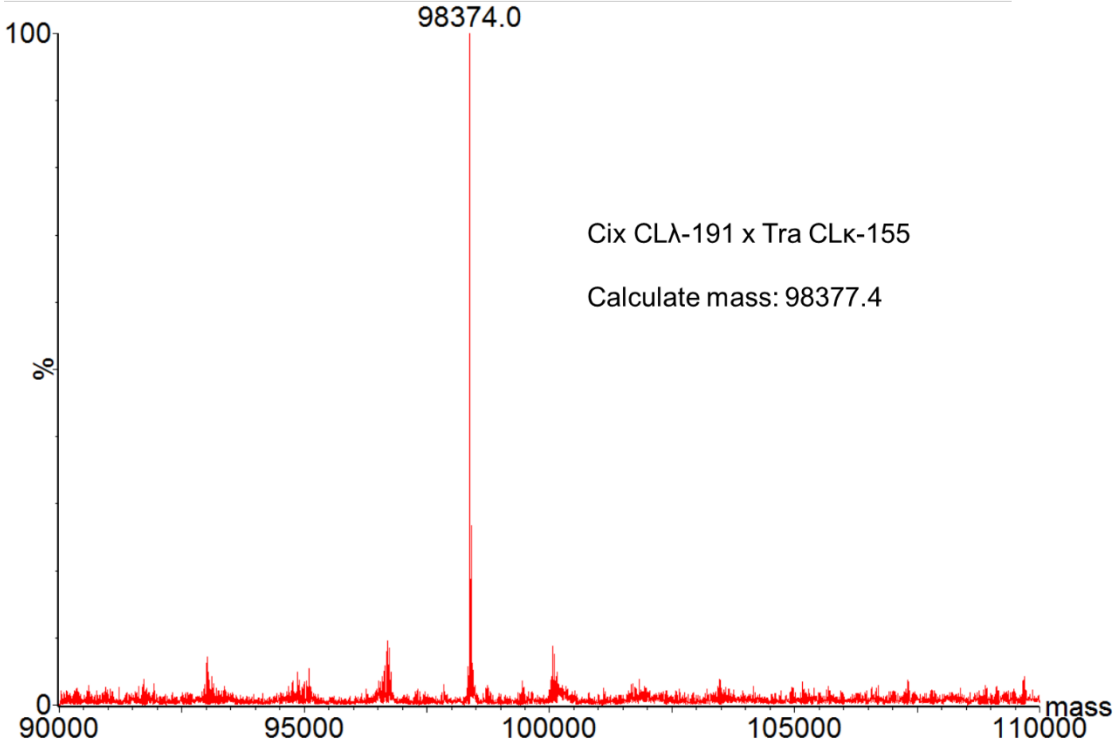
98374.0
100
%
0
Cix CLλ-191 x Tra CLκ-155
Calculate mass: 98377.4
90000
95000
100000
105000
110000
mass

E)

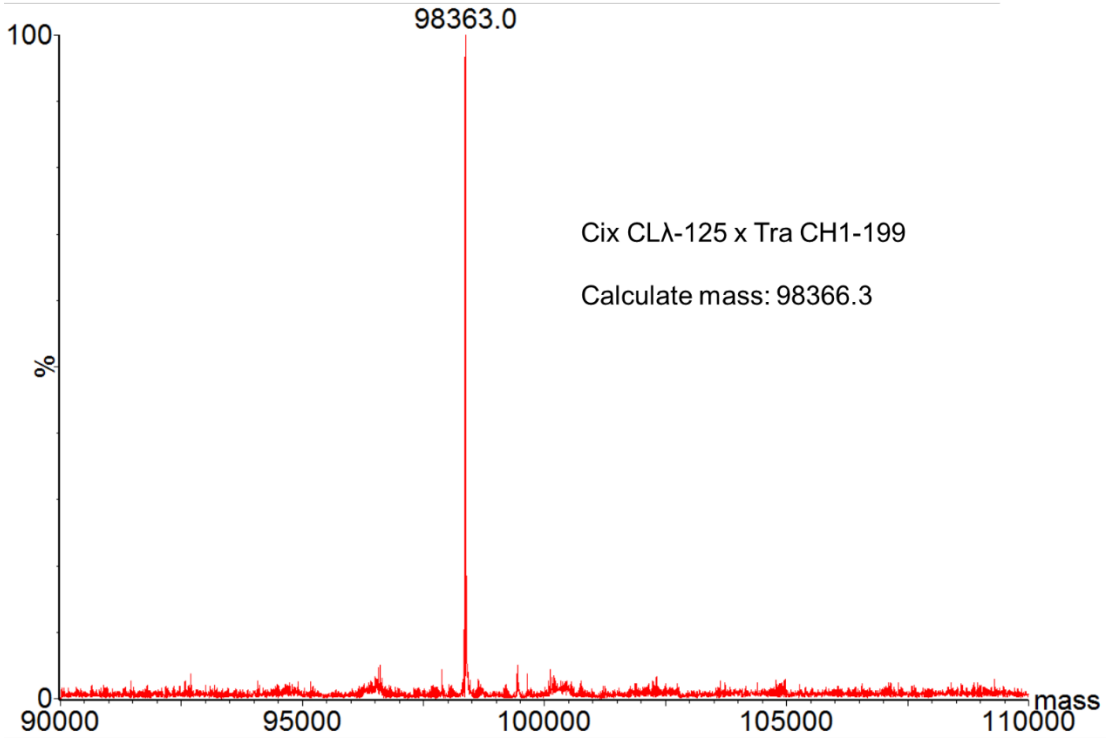
98363.0
100
%
0
Cix CLλ-125 x Tra CH1-199
Calculate mass: 98366.3
90000
95000
100000
105000
110000
mass

F)

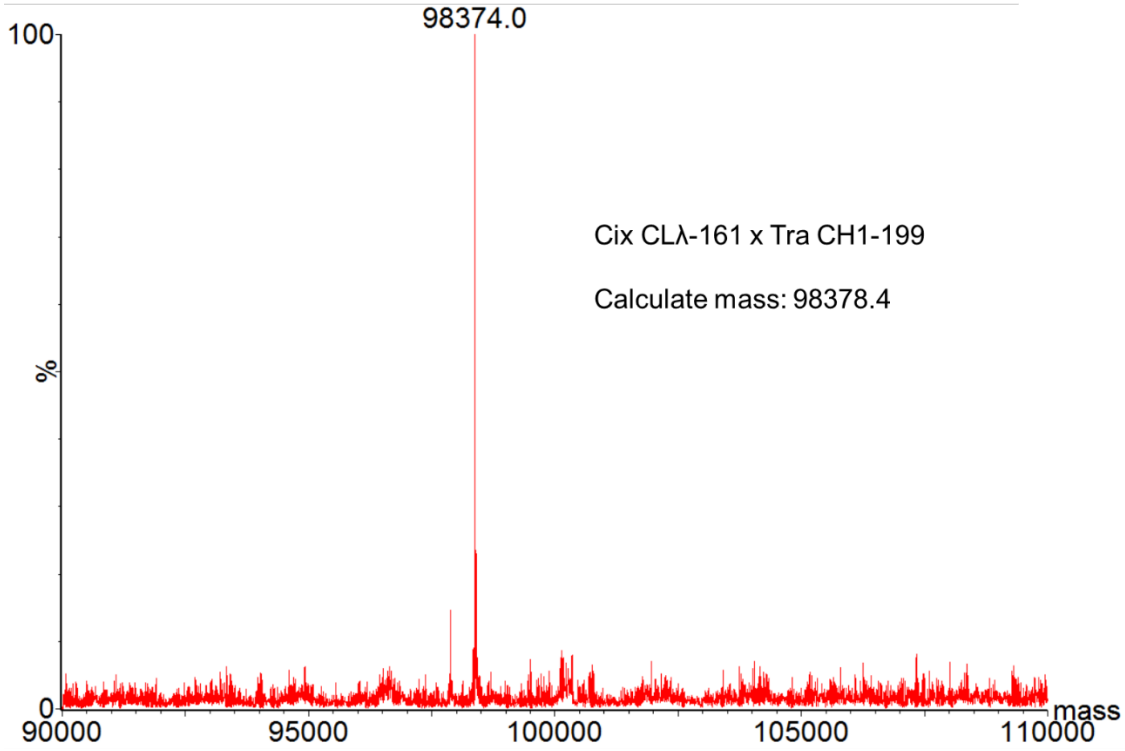
98374.0
100
%
0
Cix CLλ-161 x Tra CH1-199
Calculate mass: 98378.4
90000
95000
100000
105000
110000
mass

G)

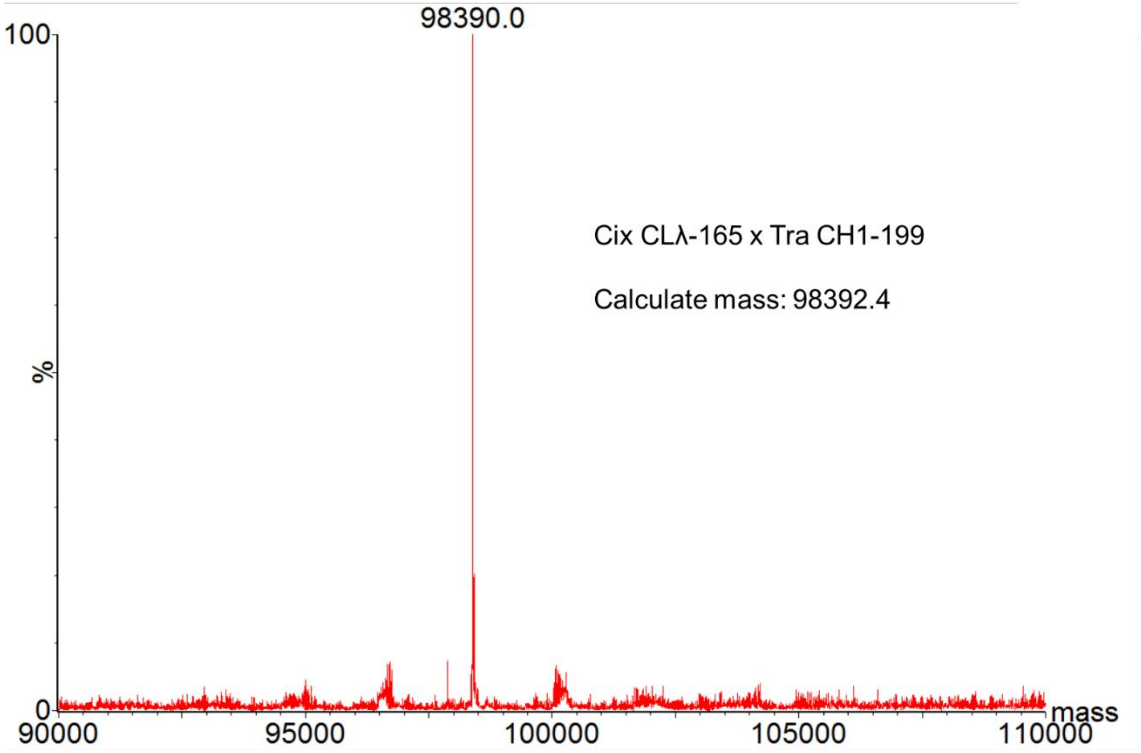
98390.0
100
%
0
Cix CLλ-165 x Tra CH1-199
Calculate mass: 98392.4
90000
95000
100000
105000
110000
mass

H)

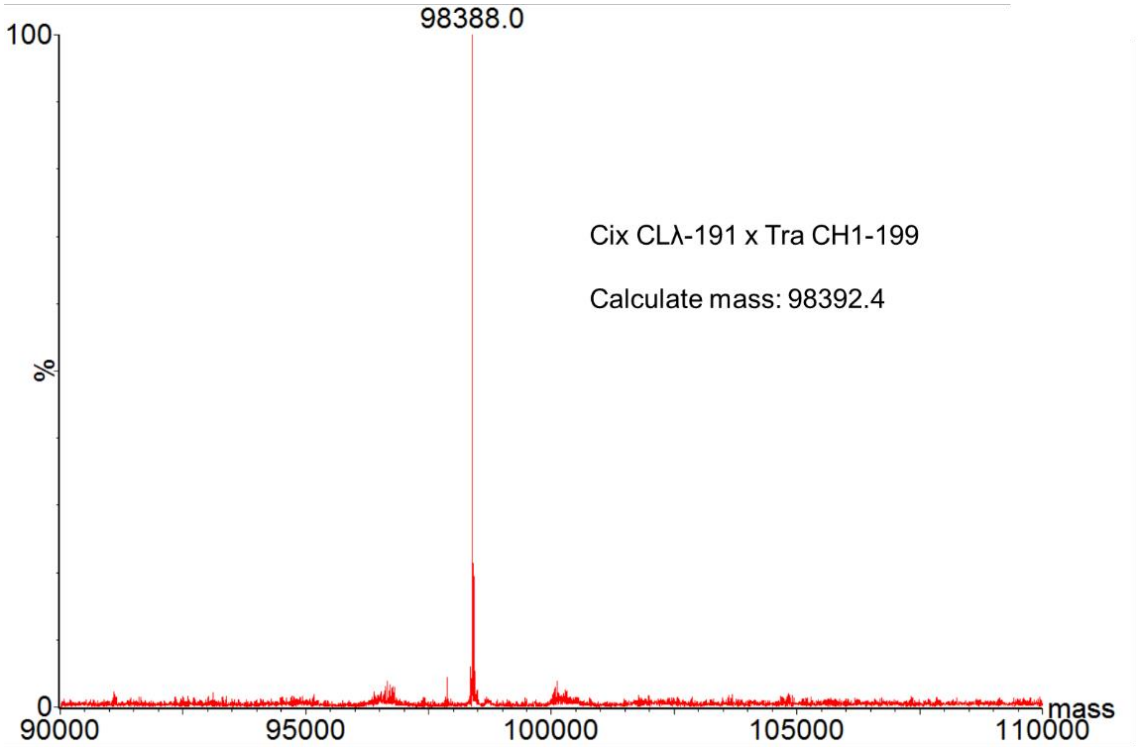
98388.0
100
%
0
Cix CLλ-191 x Tra CH1-199
Calculate mass: 98392.4
90000
95000
100000
105000
110000
mass

Figure 16. MS checks of the prepared Cix×Tra bispecific Fab-dimers.

MS analyses of eight combinations of the Fab-dimers. CLλ-125, CLλ-161, CLλ-165, and CLλ-191 combined with Tra-Fab CLκ-155 (A to D, respectively) and CLλ-125, CLλ-161, CLλ-165, and CLλ-191 combined with Tra-Fab CH1-199 (E to H, respectively).

CH1, first constant region of the heavy chain; Cix, cixutumumab; CLκ, κ light chain constant region; CLλ, λ light chain constant region; Fab, antigen-binding fragment; MS, mass spectrometry; Tra, trastuzumab.

Table 3. MS analyses of Tra×Cix Fab-dimers.

Fab-dimer	Calculated mass (Da)	Observed mass (Da)
Cix-CLλ-125 x Tra-CLκ-155	98351.4	98349.0
Cix-CLλ-161 x Tra-CLκ-155	98363.4	98361.0
Cix-CLλ-165 x Tra-CLκ-155	98377.4	98374.0
Cix-CLλ-191 x Tra-CLκ-155	98377.4	98374.0
Cix-CLλ-125 x Tra-CH1-199	98366.3	98363.0
Cix-CLλ-161 x Tra-CH1-199	98378.4	98374.0
Cix-CLλ-165 x Tra-CLκ-155	98392.4	98390.0
Cix-CLλ-191 x Tra-CLκ-155	98392.4	98388.0

CH1, first constant region of the heavy chain; Cix, cixutumumab; CLκ, κ light chain constant region; CLλ, λ light chain constant region; Fab, antigen-binding fragment; MS, mass spectrometry; Tra, trastuzumab.

A)

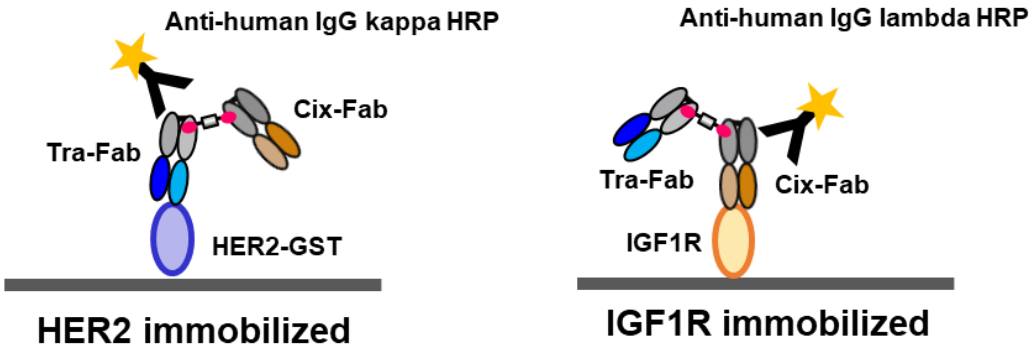
Anti-human IgG kappa HRP
Cix-Fab
Tra-Fab
HER2-GST
HER2 immobilized
Anti-human IgG lambda HRP
Tra-Fab
Cix-Fab
IGF1R
IGF1R immobilized

B)

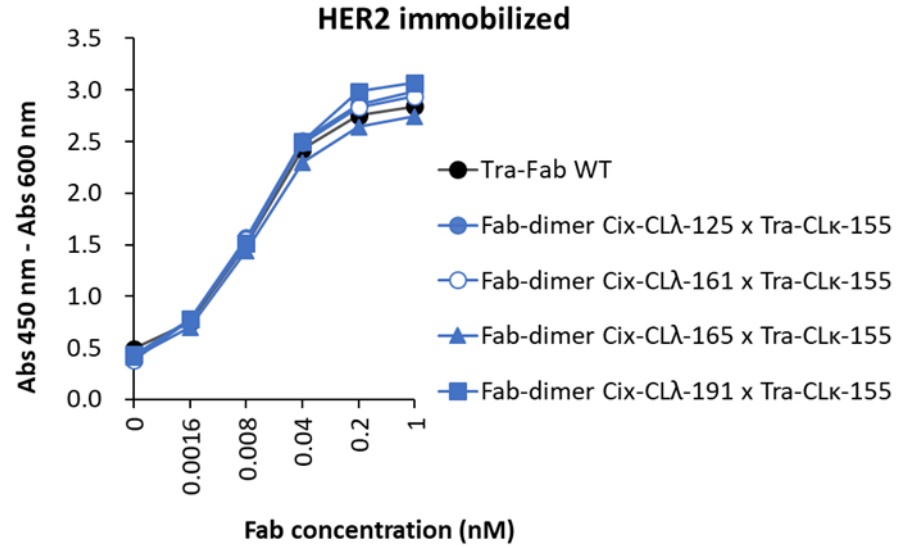
HER2 immobilized
Abs 450 nm - Abs 600 nm
3.5
3.0
2.5
2.0
1.5
1.0
0.5
0.0
0
0.0016
0.008
0.04
0.2
1
Fab concentration (nM)
Tra-Fab WT
Fab-dimer Cix-CLλ-125 x Tra-CLκ-155
Fab-dimer Cix-CLλ-161 x Tra-CLκ-155
Fab-dimer Cix-CLλ-165 x Tra-CLκ-155
Fab-dimer Cix-CLλ-191 x Tra-CLκ-155

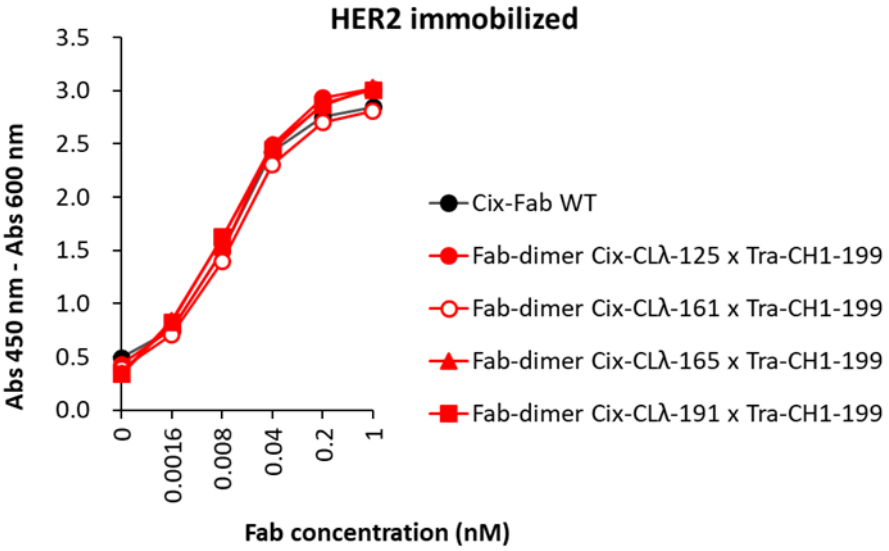
HER2 immobilized
Abs 450 nm - Abs 600 nm
3.5
3.0
2.5
2.0
1.5
1.0
0.5
0.0
0
0.0016
0.008
0.04
0.2
1
Fab concentration (nM)
Cix-Fab WT
Fab-dimer Cix-CLλ-125 x Tra-CH1-199
Fab-dimer Cix-CLλ-161 x Tra-CH1-199
Fab-dimer Cix-CLλ-165 x Tra-CH1-199
Fab-dimer Cix-CLλ-191 x Tra-CH1-199

2

C)

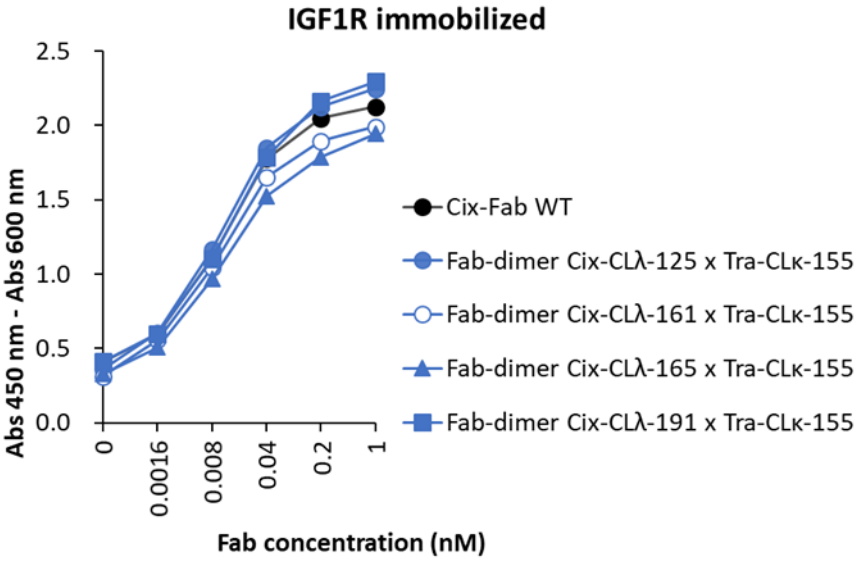

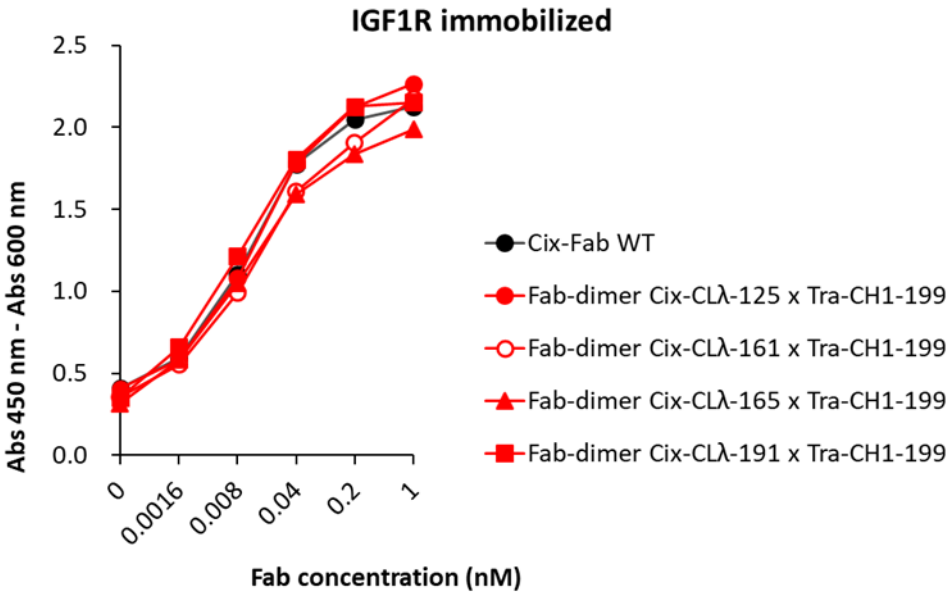

Figure 17. Binding activity analysis by ELISA for Cix×Tra Fab-dimers prepared using indicated variants.

(A) Schematic image of ELISA assays used to analyze the binding activity to HER2

and IGF1R of Cix×Tra Fab-dimers.

(B, C) ELISA analysis results of the binding activity of Cix×Tra Fab-dimers for each antigen, HER2 and IGF1R.

CH1, first constant region of the heavy chain; Cix, cixutumumab; CLκ, κ light chain constant region; CLλ, λ light chain constant region; ELISA, enzyme-linked immunosorbent assay; Fab, antigen-binding fragment; GST, glutathione S-transferase; HER2, human epidermal growth factor receptor 2; HRP, horseradish peroxidase; Ig, immunoglobulin; IGF1R, insulin-like growth factor-1 receptor; Tra, trastuzumab; WT, wild-type.

4.6 Growth Inhibition Activity of anti-HER2×anti-IGF1R Bispecific Fab-Dimers

It has been demonstrated that IGF1R and HER2 display important signaling interactions in breast cancer [51-53]. Dual-targeting IGF1R and HER2 resulted in synergistic growth inhibition of BT-474, an IGF1R- and HER2-overexpressing breast cancer cell line [54, 55]. We used this cell line to analyze the cytotoxic activity of Cix×Tra Fab-dimers. We confirmed that that there was no or little growth inhibition from Cix-Fab or Tra-Fab alone and in combination. However, the addition of Cix×Tra Fab-dimers significantly enhanced growth inhibition in a dose-dependent manner. All eight combinations of Cix×Tra Fab-dimers showed similar growth inhibition activities. Fab-dimers consisting of Cix×control Fab (anti-dinitrophenyl) showed no inhibition activity (Figure 18).

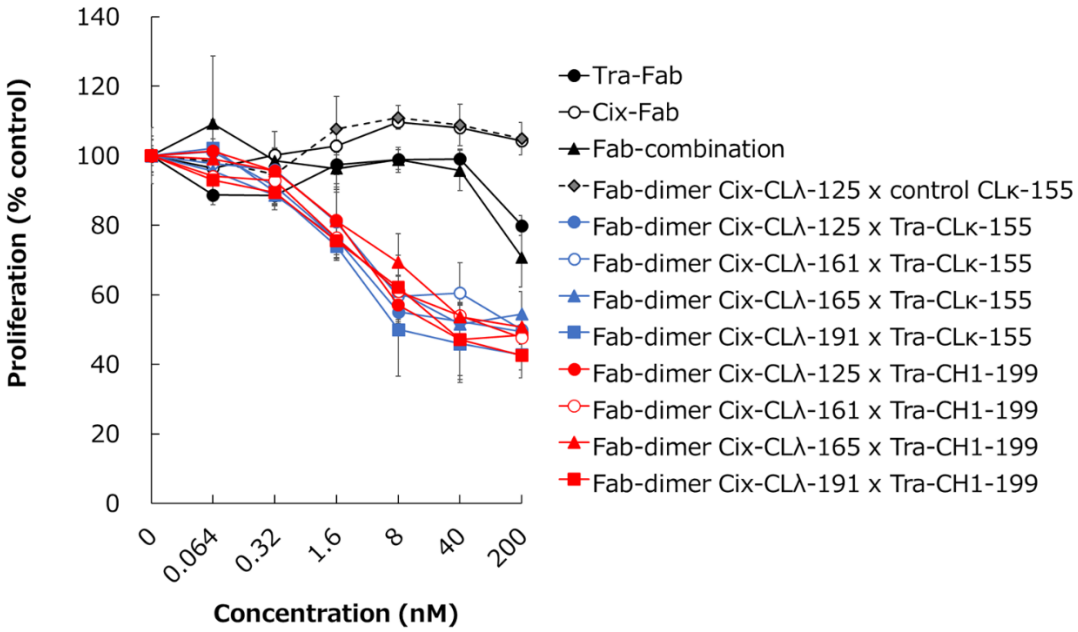

Figure 18. The antagonistic activity of Cix×Tra Fab-dimers.

Influence of the indicated molecules on proliferation of the HER2- and IGF1R-overexpressing breast cancer cell line BT-474. All eight combinations of the prepared Fab-dimers are shown.

CH1, first constant region of the heavy chain; Cix, cixutumumab; CLκ, κ light chain constant region; CLλ, λ light chain constant region; Fab, antigen-binding fragment; HER2, human epidermal growth factor receptor 2; IGF1R, insulin-like growth factor-1 receptor; Tra, trastuzumab.

5 Discussion

5.1 Identification of Highly Reactive Positions in CLλ for Efficient Chemical Conjugation

In this study, we first identified multiple positions supporting efficient *o*-Az-Z-Lys incorporation and chemical conjugation in the antibody CLλ domain by an extensive survey using the RF-1–knockout *E. coli* W3110 strain. Only a few positions in Fab domains have been used for chemical conjugation using nnAAs, even in CH1 and CLκ, mainly due to restrictions on conjugation-site selection [16, 17, 19, 21, 22]. One restriction was the vulnerability of the amber-suppression method to the sequence context surrounding the incorporation site for an nnAA. To avoid this problem, in our previous study, we decided to redefine the UAG stop codon in the W3110 strain, which is an appropriate strain for expression of Fab molecules [18], by generating an RF-1 knockout of this strain [6]. The *in vivo* translation definition of UAG has been successfully changed to *o*-Az-Z-Lys by expressing the archaeal pair of $tRNA^{Pyl}$ and an *o*-Az-Z-Lys–specific variant of pyrrolysyl-tRNA synthetase mutant (PylRS Y306A and Y384F) in the RF-1–knockout W3110 strain. Supplementation of *o*-Az-Z-Lys in the culture medium resulted in the exclusive incorporation of *o*-Az-Z-Lys at the UAG position in Fab molecules [6]. Another restriction is related to the degree of solvent exposure in a position as represented by the ASA ratio. Conjugation sites were previously selected among positions with high solvent exposure, typically positions with ASA ratio values ≥0.4, because conventional nnAAs such as *p*-AcF or *p*-AzF have relatively shorter side chains than pyrrolysyl derivatives such as *o*-Az-Z-Lys; therefore, they must be introduced at high solvent-exposure positions [56]. In our previous study, we examined whether these restrictions could be overcome by

using the RF-1–knockout W3110 *E. coli* strain and *o*-Az-Z-Lys with a flexible long side chain. We examined 42 positions in the CH1 and CLκ domains for replacement to *o*-Az-Z-Lys and checked their reactivity during SPAAC and confirmed that all position variants could be expressed avoiding ‘‘sequence context,’’ and most of the examined positions with middle ASA ratios (0.2 to 0.4) support highly efficient conjugation and exhibit reactivities ranging from 80% to 90%. Furthermore, the X-ray crystallographic study clearly illustrated that *o*-Az-Z-Lys with a long side chain was highly reactive owing to being exposed on the Fab molecule surface, while *p*-AzF introduced at the same position exhibited significantly limited reactivity due to interference of the surrounding amino acid side chains [6]. These results demonstrated that the ‘‘sequence context,’’ vulnerability of the amber-suppression method and the restriction of position selection related to solvent exposure were greatly overcome using the RF-1–knockout W3110 *E. coli* strain and *o*-Az-Z-Lys. These results particularly encouraged us to survey the CLλ with a similar strategy in addition to CH1 and CLκ constant regions.

In this study, we selected 20 positions exhibiting ASA ratio values between 0.2 and 0.4 and examined *o*-Az-Z-Lys reactivity in these variants during SPAAC using the DIBO-Alexa Fluor 488 dye as a model payload. Overall, 13 of 16 positions exhibited high reactivities of more than 80%, although the reactivity of four positions (CLλ 151, 171, 210, and 213) could not be evaluated because of significantly lower yields. This result demonstrated that the positions with moderate ASA ratio values between 0.2 and 0.4 have an intensive tendency to support effective chemical conjugation, consistent with our previous study focused on CH1 and CLκ constant regions. Furthermore, these variants mostly showed the same antigen-binding activity and

thermal stability, suggesting that the incorporation of *o*-Az-Z-Lys did not affect the overall conformational structure of Cix-Fab molecules, despite the fact that *o*-Az-Z-Lys has a long and bulky side chain compared with natural amino acids. Similar results were obtained in our previous X-ray crystallographic study. The *o*-Az-Z-Lys–containing Tra-Fab structure illustrated that the bulky azidobenzyl moiety of *o*-Az-Z-Lys protruded from the Fab molecule surface, and the whole structure superimposed well on the reported structures of the Fab fragments of anti-HER2 antibody 4D5 (PDB IDs: 5TDP and 5TDN), IgG HC (PDB ID: 4UB0), and humanized anti–P185-HER2 antibody 4D5 (PDB ID: 1FVD) [6]. Although we did not perform X-ray crystallographic analysis in this study, *o*-Az-Z-Lys may have been introduced into CLλ positions in a similar manner and consequently had minimal effects on the Cix-Fab overall conformational structure and antigen-binding affinity.

The optimal mutation sites on CLλ for preparation of ADCs or protein conjugates such as bispecific antibodies have not been explored yet. For example, Lyu et al reported only three positions (CLλ 155, 193, and 202) for incorporation of the nnAA p-AcF and efficient drug conjugation; however, they performed the variant synthesis under the limitations of the amber-suppression method and solvent exposure and have not reported any other positions [57]. Thus, the use of the RF-1–knockout W3110 *E. coli* strain and *o*-Az-Z-Lys must have increased the number of available positions in the CLλ for conjugation. The genetic incorporation of UAAs not only allows us to site-specifically modify the protein surface but also facilitates our exploration of various Fab and IgG conjugates with different geometries. The multiple positions identified in this study allow the generation of homogeneous ADCs and chimeric proteins in various geometries that cannot be formed by genetic

fusion approaches.

5.2 Preparation and *In vitro* Cytotoxic Activity of Fab-Drug Conjugates

We demonstrated that the homogeneous Cix-Fab–DM1 conjugates could be prepared efficiently using the selected representative four positions (CLλ 125, 161, 165, and 191), and all Cix-Fab–DM1 conjugates exhibited almost the same antigen-binding activity. Cysteine has generally been used for site-specific conjugations [18, 23, 58, 59] but may induce the deactivation of proteins, especially antibody fragments. The genetic incorporation of *o*-Az-Z-Lys and the click-chemistry reaction used in this study guaranteed the site-specific conjugation, which could be achieved without compromising the antigen-binding activity.

In cytotoxicity assays, our Cix-Fab–DM1 conjugates required the anti–human CLλ antibody as the cross-linking reagent to induce formation of the bivalent Cix-Fab complex leading to internalization of Cix-Fab–DM1 conjugates. The parent Cix-IgG is a bivalent molecule, and hence it has been reported that Cix induces IGF1R dimerization and significant internalization [47]. Although we confirmed the availability of the incorporated *o*-Az-Z-Lys for efficient conjugation using Cix-Fab, this monovalent molecule has a limitation in the accurate estimation of efficacy and potency of cytotoxic activity of Cix-Fab–DM1 conjugates since the efficiency of dimerization of the Cix-Fab–DM1 conjugate induced by the cross-linker could not be assessed. On the other hand, the *o*-Az-Z-Lys–incorporated Cix-based variants expressed as IgG and conjugated DM1 may exhibit cytotoxicity without the cross-linking reagent. *O*-Az-Z-Lys–incorporated IgG molecules could be expressed using

the mammalian cell expression system consisting of $tRNA^{pyl}$ and *o*-Az-Z-Lys–specific variant of pyrrolysyl-tRNA synthetase mutant (PylRS Y306A and Y384F), the same pair used in the W3110 RF-1–knockout strain [57]. In our previous study, we demonstrated that full-length Tra-IgG incorporated with *o*-Az-Z-Lys in CH1 or CLκ could be expressed taking advantage of this system in HEK293 cells and efficiently conjugated DBCO-Alexa488 as the model payload by SPAAC reaction. Recently, it has been reported that an IGF1R-targeted ADC, designed by anti-IGF1R IgG (hz208F2-4)–conjugated auristatin, showed highly potent cytotoxic effect on IGF1R-overexpressing tumor cells [60]. To determine the extent of cytotoxic activity of ADCs prepared using our *o*-Az-Z-Lys–containing Cix-IgG–based variants, further studies are needed.

Most of the ADCs in clinical and preclinical development are based on the whole IgG format [61]; however, treatment of solid tumors with large macromolecules remains a risk and a challenge [62, 63]. On the other hand, smaller formats, including Fabs, may be ideal as ADC cancer therapeutics because they could have higher tumor uptake, a better tumor-to-blood ratio, and faster clearance than full-length IgG antibodies [64-66]. Furthermore, Fabs do not have the Fc region, which could be beneficial to overcome potential effector function–related toxicities [67, 68]. Using the monomethyl auristatin E (MMAE) payload, an anti-HER2 Tra-Fab conjugate exhibited potent antitumor activity *in vitro* and *in vivo* in a cancer model [69]. While that conjugate was prepared by reduction of a disulfide bond in Fab and MMAE conjugation during re-bridging, our strategy using *o*-Az-Z-Lys facilitates the efficient generation of Fab-drug conjugates without such complex methods.

In this study, we conjugated a cytotoxic reagent DM1 as the model antitumor agent.

However, these next-generation technologies are now being used beyond cytotoxin-conjugated ADCs. These site-specific conjugations have been applied for the generation of many different immunoconjugates, including immunosuppressive antibodies [70, 71] and antibody-antibiotic conjugates [72]. Alternatively, ADCs are used in diagnosis and imaging. The recent advancements in positron emission tomography (PET) and optical imaging (OI) resulted in great interest in the development of multimodal PET/OI probes that can be employed during the diagnosis, staging, and surgical treatment of cancer [73]. The combination of PET/OI agents with antibodies using site-specific conjugations would enhance both the sensitivity and selectivity. Multimodal PET/OI and radiolabeled immunoconjugates have been developed by the site-specific labeling of antibody N297 glucan using chemo-enzymatic strategy [74-76]. In another study, the site-specific DNA-antibody conjugates were used for specific and sensitive immuno-polymerase chain reaction (PCR) used as diagnosis and imaging [77]. In these applications, Fabs are thought to be the optimal format because of their higher tumor penetration, better tumor-to-blood ratio, and faster clearance.

Antibodies and Fabs can be used to modify the surface of nanoparticles and other biomedical materials such as biosensors for enhanced target binding. The site-specific conjugation enables installation onto the surface in a controlled manner without attenuation of the binding activity. Fab-conjugated polymeric micelles of appropriate density and geometry of Fab molecules have shown increased cell uptake and potency compared with nontargeted micelles [78]. As control of protein immobilization is important, site-directed mutagenesis and immobilization using site-specific conjugation could improve the biosensor performance [79].

The site-specific modification strategy through incorporation of appropriate nnAAs in Fab achieves generation of homogeneous conjugates. The optimal positions in CH1, CLκ, and CLλ regions identified in this and our previous study allows the generation of payload conjugates using both IgGκ and CLλ antibodies; therefore, this is a powerful approach to generate many types of ADCs, Fab-drug conjugates, Fab-conjugated nanoparticles, and other biomedical materials for therapeutics, diagnosis, imaging, biosensing, and biomedical implantation.

5.3 Generation of Bispecific Fab-Dimers and Activity Analysis

The genetic incorporation of nnAAs and bio-orthogonal chemical conjugation not only allows us to site-specifically modify the protein surface but also facilitates our exploration of various Fab conjugates with different combination and geometries. We generated eight combinations of Cix×Tra Fab-dimers. Notably, their binding activity to both antigens (HER2 and IGF1R) was not affected by Fab-dimerization. Our *in silico* simulation demonstrated that the distance between the two Fabs in the Fab-dimer prepared using the DBCO-PEG4-DBCO linker was adequate and similar to that of two Fabs in native IgG molecules (data not shown); therefore, the affinity decrease due to steric hindrance arising from interaction of two Fabs in the Fab-dimer could be avoided. The length of DBCO-PEG-DBCO linkers is flexible and can be adjusted for each Fab-dimer. We have prepared a series of linkers that have different PEG lengths (PEG_1 to PEG_{25}). However, how short the linkers can be without an affinity decrease should be determined for each Fab-dimer molecule.

The Cix×Tra Fab-dimers we prepared significantly enhanced the growth inhibition of the parent Cix-Fab in a dose-dependent manner. Overexpression of HER2 and

IGF1R may promote the formation of a HER2/IGF1R heterodimer [80]. Indeed, the existence of HER2/IGF1R complexes in breast cancer cell lines could improve the efficacy of Tra *in vitro* [81]. Bispecific Cix×Tra Fab-dimers are thought to be more potent than the combination of Fabs alone because they bind HER2 and IGF1R of the same heterodimer molecule simultaneously and bind more strongly by the avidity effect; therefore, they inhibit signals from the heterodimer effectively. These results indicate that bispecific Fab-dimers could have a unique function beyond that of Fab-monomers dimerized using chemical conjugation.

While this study demonstrates the generation of antagonists by Fab-dimers, this general strategy can be applied for other purposes. In fact, other than our study, another group also previously reported an HER2 agonist by controlling the relative orientation of Tra-Fab-dimers [6, 82, 83]. Our approach can be used for screening broadly to discover antagonists and agonists of cytokine and growth factor receptors.

As opposed to blocking pathogenic signaling by inhibitory antibodies, some therapeutic concepts require the activation of receptor signaling by agonistic antibodies. Bispecific antibodies are particularly suitable to activate multicomponent receptor complexes in which concurrent binding of a receptor and coreceptor is required for activation. The most prominent example of the mimetics of endogenous growth factor is the fibroblast growth factor 21 (FGF21)–mimetic bispecific antibody [84]. Activation of the FGF21 pathway has been reported to ameliorate obesity and diabetes [85, 86]. However, the recombinant FGF21 has poor pharmacokinetic properties. Therefore, an agonistic bispecific antibody BFKB8488A (Roche) has been designed to activate this metabolic pathway by selectively targeting the fibroblast growth factor receptor 1C (FGFR1C)–β-klotho (KLB) receptor complex

[84]. Preliminary results from an ongoing first-in-human trial showed an improvement of the cardio-metabolic profile in obese subjects with insulin resistance [87]. Surrogate Wnt agonists are also noteworthy. Wnt proteins modulate cell proliferation and differentiation and the self-renewal of stem cells by inducing β-catenin–dependent signaling through the Wnt receptor frizzled (FZD) and the coreceptors LRP5 and LRP6 to regulate cell fate decisions and growth and repair of several tissues. Wnt proteins are highly hydrophobic and require detergents for purification, which prevents the use of Wnt proteins as therapeutic agents. Therefore, water-soluble bispecific molecules were developed, which induced FZD-LRP5/LRP6 heterodimerization and input canonical Wnt and β-catenin signaling [88]. Although these bispecific antibodies phenocopied the natural endogenous ligand canonical signaling, the potency was significantly weaker than that of the endogenous ligand. The importance of geometry, orientation, and proximity of the cytokine receptor complex has been profoundly studied using the erythropoietin (EPO) receptor [89]. In this type-I transmembrane receptor signaling, receptor homodimerization is the essential step, similar to most cytokine and growth factor receptors [90]. A series of geometrically controlled ligands to the EPO receptor were designed based on the high-affinity designed ankyrin repeat protein (DARPin) binder using structural modeling, which can systematically control EPO receptor dimerization orientation and distance between monomers. The crystal structure analysis revealed that EPO receptor dimer geometries by varying the intermonomer angle and distance corelated with full, partial, and biased agonistic activity. The optimized designed ligand showed similar activity to that of the native EPO [89]. This “topological tuning” may be attributed to altered intracellular orientations of

Janus kinase 2 (JAK2) relative to its substrates or mechanical distortion that leads to changes in complex stability and receptor internalization. This approach can be used to identify agonistic molecules with therapeutically desirable signaling outputs not only for homodimeric receptors such as the EPO receptor but also for heterodimeric receptors such as those from the common β and common γ receptor families [91, 92].

The approach based on the DARPin format mentioned above has some limitations. First is the limitation of structural diversity of DARPin-dimers due to the restriction of the angle and distance achieved by DARPin engineering. Second, DARPin engineering was performed by adjusting the ankyrin repeat numbers so that the angle and distance changed simultaneously. This makes it difficult for precise optimization of the DARPin-dimer structure. Third, although the DARPin format is stable in itself [93], the DARPin-dimers were formed by noncovalent bonding; therefore, the therapeutic application of the optimized molecule with high potency seems difficult.

We have identified a number of positions supporting efficient conjugation. Overall, 16 positions in CH1, 19 positions in CLκ, and 13 positions in CLλ guaranteed more than 80% SPAAC reactivity. The relative Fab orientation in the Fab-dimer can be controlled by the position selection for the linkage of the two Fabs. Furthermore, the length of the chemical linker used for Fab-dimer preparation is highly flexible. Therefore, the structural diversity of the Fab-dimer is determined by the combination of position selections of the two Fabs and the linker length. Furthermore, we have developed the method for one-pot synthesis of a wide variety of Fab-dimer libraries in a high-throughput, combinatorial manner. These high-content Fab-dimer libraries would enable “topological tuning,” identification of the potent Fab-dimers with therapeutically desirable signaling outputs, and further optimization by adjusting the

orientation and distance of two Fabs independently. Fab-dimers generated taking advantage of *o*-Az-Z-Lys and the SPAAC reaction contain a stable covalent bond. Hence, they would be expected to have a desirable stability for therapeutic development. We did not perform *in vivo* analysis using the Fab-dimer in this study. To determine the extent of *in vivo* stability or pharmacokinetics, further *in vivo* studies are needed.

Besides mimicking endogenous ligands such as cytokines or growth factors, agonistic bispecific antibodies can induce novel therapeutic effects by linking the appropriate two targets located on the surface of pathogenic cells. The bispecific molecules engaging the inhibitory Fcγ receptor (FcγR) FcγRIIb (CD32B) to CD79B, the signal transduction molecule in the B-cell receptor (BCR) complex, negatively regulated B-cell activation with disruption of signal transduction and attenuation of BCR-induced calcium mobilization, proliferation, and pathogenic Ig secretion [94]. Similarly, the activation of human pathogenic mast cells was potently inhibited by engagement of CD300a, an inhibitory receptor to IgE, due to the inhibition of the signaling events induced by FceRI, an IgE receptor [95]. Moreover, it has recently been reported that engineered synthetic cytokines drive formation of novel cytokine receptor dimer pairings that are not formed by endogenous cytokines and that are not found in nature, and which activate distinct signaling pathways [96]. This concept enables the full combinatorial scope of dimeric signaling receptors to be exploited for basic research and drug discovery. Bispecific antibodies seem to be particularly suitable for such research; however, most of the bispecific antibody formats compatible to combinatorial formation require two Fabs sharing a common LC [97]. Obtaining antibodies with common LC for various receptors is highly laborious and

time consuming. This limitation makes it difficult to perform the exploration of receptor pairing with therapeutically desirable signaling output in a large scale and for a wide range of targets.

We demonstrated that our strategy enables the generation of bispecific Fab-dimers composed of two Fabs with different LCs, albeit with different LC constant regions—CLκ and CLλ—expressed and purified independently. The generation of a wide variety of bispecific antibodies in a combinatorial "off-the-shelf" manner provides the opportunity to discover the novel receptor pairing with therapeutically desirable signaling output properties.

6 Conclusion

In the present study, we showed that *o*-Az-Z-Lys could be incorporated with high reactivity in antibody CLλ positions. Experiments utilizing the four representative positions demonstrated the utility of the newly identified positions for generation of Fab-drug conjugates and bispecific Fab-dimers. These results showed that our approach greatly enhanced the availability of both IgGκ and IgGλ isotypes, thereby providing an efficient method to generate antibody-based therapeutic molecules, including bispecific antibodies, without LC isotype limitation (Figure 19). We have described the bispecific Fab-dimer molecules composed of IgGκ and IgGλ combinations that could be prepared in a one-pot manner, which exhibit large degrees of flexibility in their relative orientation and distance between the two Fab molecules conjugated to one another. These results opened up a way to prepare a library containing a wide variety of bispecific Fab-dimers and discover antagonists and agonists with therapeutically desirable signaling output properties for cytokine and growth factor receptors.

A)

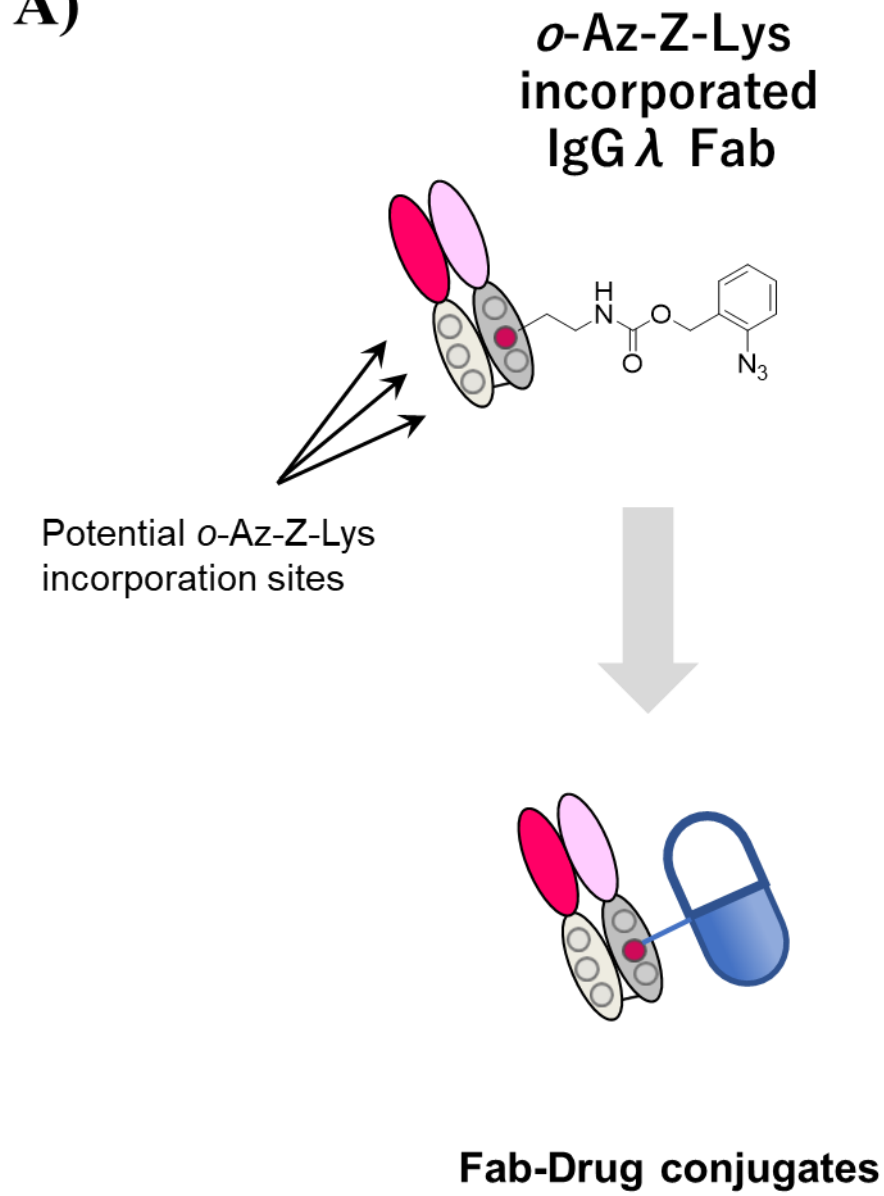
o-Az-Z-Lys
incorporated
IgG λ Fab
H
N
O
O
N_3
Potential *o*-Az-Z-Lys
incorporation sites
Fab-Drug conjugates

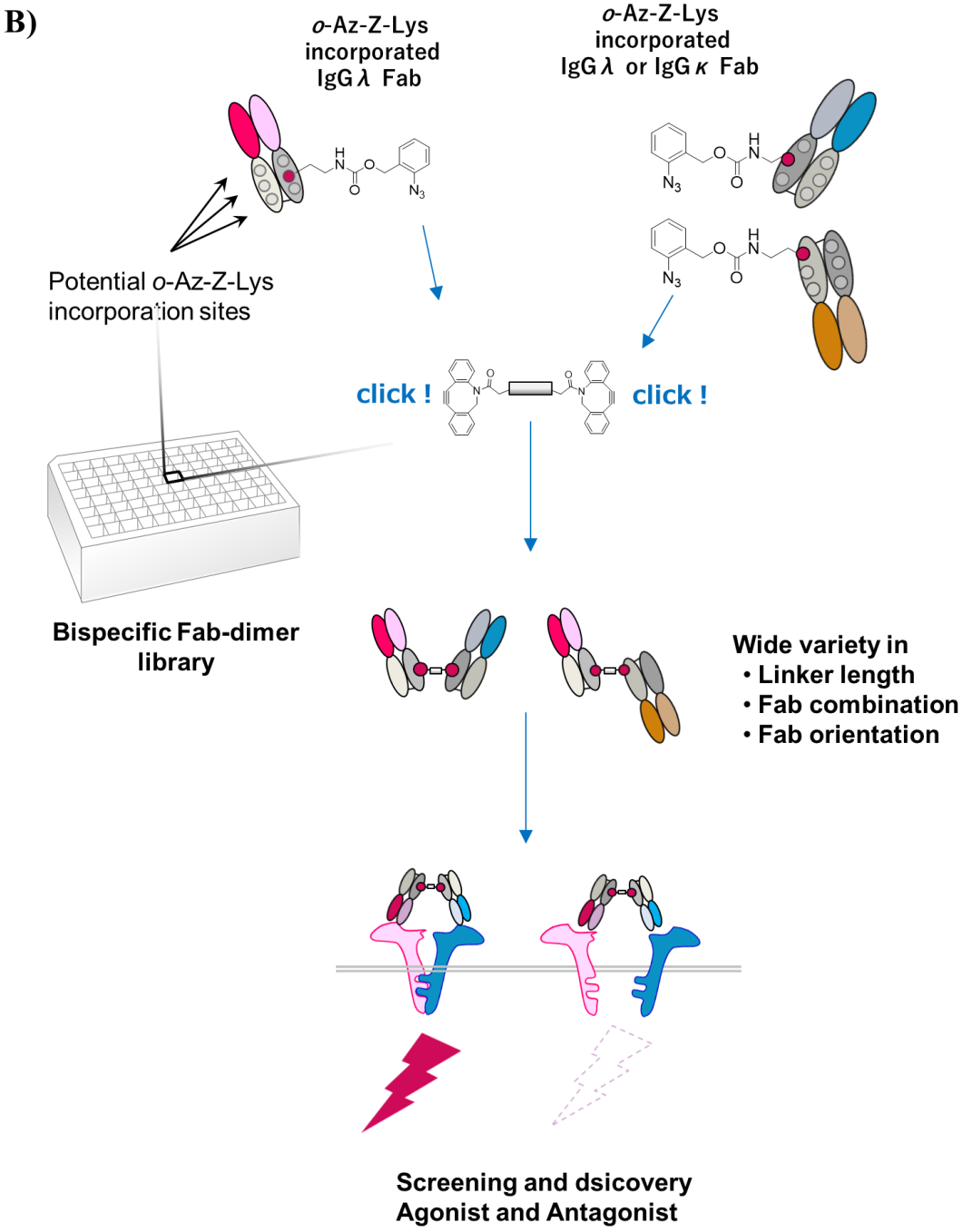

Figure 19. Expected future directions for various Fab conjugates utilizing bio-

orthogonal chemistry using expanded genetic code.

A) Fab-drug conjugates for therapy and diagnosis.

B) Drug discovery of antagonist or agonist against cytokines or growth factors and with desired therapeutic activity optimized by "topological tuning."

Fab, antigen-binding fragment; Ig, immunoglobulin; *o*-Az-Z-Lys, *N*ε-(*o*-Azidobenzyloxycarbonyl)-L-lysine.

7 References

1. Edelman GM (1959) Dissociation of γ-globulin. *Journal of the American Chemical Society* 81:3155–3156.
   doi: 10.1021/ja01521a071
2. Alzari PM, Lascombe MB, Poljak RJ (1988) Three-dimensional structure of antibodies. *Annual Review of Immunology* 6:555–580.
   doi: 10.1146/annurev.iy.06.040188.003011
3. Song A, Myojo K, Laudenslager J, et al (2014) Evaluation of a fully human monoclonal antibody against multiple influenza A viral strains in mice and a pandemic H1N1 strain in nonhuman primates. *Antiviral Research* 111:60–68.
   doi: 10.1016/j.antiviral.2014.08.016
4. Liu H, Chumsae C, Gaza-Bulseco G, et al (2010) Ranking the susceptibility of disulfide bonds in human IgG1 antibodies by reduction, differential alkylation, and LC−MS analysis. *Analytical Chemistry* 82:5219–5226.
   doi: 10.1021/ac100575n
5. Montaño RF, Morrison SL (2002) Influence of the isotype of the light chain on the properties of IgG. *The Journal of Immunology* 168:224–231.
   doi: 10.4049/jimmunol.168.1.224
6. Kato A, Kuratani M, Yanagisawa T, et al (2017) Extensive survey of antibody invariant positions for efficient chemical conjugation using expanded genetic codes. *Bioconjugate Chemistry* 28:2099–2108.
   doi: 10.1021/acs.bioconjchem.7b00265
7. Mckian KP, Haluska P (2009) Cixutumumab. *Expert Opinion on Investigational Drugs* 18:1025–1033.

doi: 10.1517/13543780903055049

8. Orfila C, Rakotoarivony JL, Manuel Y, Suc J-M (1988) Immunofluorescence characterization of light chains in human nephropathies. *Virchows Archiv. A, Pathological Anatomy and Histopathology* 412:591–594.
   doi: 10.1007/bf00844295
9. Lefranc M-P (2009) Antibody databases and tools: The IMGT® experience. In: *Therapeutic Monoclonal Antibodies: From Bench to Clinic* 91–114.
   doi: 10.1002/9780470485408.ch4
10. Woloschak GE, Krco CJ (1987) Regulation of kappa/lamda immunoglobulin light chain expression in normal murine lymphocytes. *Molecular Immunology* 24:751–757.
    doi: 10.1016/0161-5890(87)90058-7
11. Junutula JR, Bhakta S, Raab H, et al (2008) Rapid identification of reactive cysteine residues for site-specific labeling of antibody-Fabs. *Journal of Immunological Methods* 332:41–52.
    doi: 10.1016/j.jim.2007.12.011
12. Junutula JR, Raab H, Clark S, et al (2008) Site-specific conjugation of a cytotoxic drug to an antibody improves the therapeutic index. *Nature Biotechnology* 26:925–932.
    doi: 10.1038/nbt.1480
13. Lyons A, King DJ, Owens RJ, et al (1990) Site-specific attachment to recombinant antibodies via introduced surface cysteine residues. *Protein Engineering, Design and Selection* 3:703–708.
    doi: 10.1093/protein/3.8.703

14. Stimmel JB, Merrill BM, Kuyper LF, et al (2000) Site-specific Conjugation on serine → cysteine variant monoclonal antibodies. *Journal of Biological Chemistr*y 275:30445–30450.
doi: 10.1074/jbc.m001672200
15. Voynov V, Chennamsetty N, Kayser V, et al (2010) Design and application of antibody cysteine variants. *Bioconjugate Chemistry* 21:385–392.
doi: 10.1021/bc900509s
16. Zimmerman ES, Heibeck TH, Gill A, et al (2014) Production of site-specific antibody–drug conjugates using optimized non-natural amino acids in a cell-free expression system. *Bioconjugate Chemistry* 25:351–361.
doi: 10.1021/bc400490z
17. Tian F, Lu Y, Manibusan A, et al (2014) A general approach to site-specific antibody drug conjugates. *Proceedings of the National Academy of Sciences of the United States of America* 111:1766–1771. doi: 10.1073/pnas.1321237111
18. Shiraishi Y, Muramoto T, Nagatomo K, et al (2015) Identification of highly reactive cysteine residues at less exposed positions in the Fab constant region for site-specific conjugation. *Bioconjugate Chemistry* 26:1032–1040.
doi: 10.1021/acs.bioconjchem.5b00080
19. Kim CH, Axup JY, Dubrovska A, et al (2012) Synthesis of bispecific antibodies using genetically encoded unnatural amino acids. *Journal of the American Chemical Society* 134:9918–9921.
doi: 10.1021/ja303904e
20. Lu H, Zhou Q, Deshmukh V, et al (2014) Targeting human C-type lectin-like molecule-1 (CLL1) with a bispecific antibody for immunotherapy of acute myeloid

leukemia. *Angewandte Chemie* 53:9841–9845.

doi: 10.1002/ange.201405353

21. Axup JY, Bajjuri KM, Ritland M, et al (2012) Synthesis of site-specific antibody-drug conjugates using unnatural amino acids. *Proceedings of the National Academy of Sciences of the United States of America* 109:16101–16106.

doi: 10.1073/pnas.1211023109

22. Vanbrunt MP, Shanebeck K, Caldwell Z, et al (2015) Genetically encoded azide containing amino acid in mammalian cells enables site-specific antibody–drug conjugates using click cycloaddition chemistry. *Bioconjugate Chemistry* 26:2249–2260.

doi: 10.1021/acs.bioconjchem.5b00359

23. Shinmi D, Taguchi E, Iwano J, et al (2016) One-step conjugation method for site-specific antibody–drug conjugates through reactive cysteine-engineered antibodies. *Bioconjugate Chemistry* 27:1324–1331.

doi: 10.1021/acs.bioconjchem.6b00133.

24. Liu CC, Schultz PG (2010) Adding new chemistries to the genetic code. *Annual Review of Biochemistry* 79:413–444.

doi: 10.1146/annurev.biochem.052308.105824

25. Xu H, Wang Y, Lu J, et al (2016) Re-exploration of the codon context effect on amber codon-guided incorporation of noncanonical amino acids in Escherichia coli by the blue-white screening assay. *ChemBioChem: A European Journal of Chemical Biology* 17:1250–1256.

doi: 10.1002/cbic.201600117

26. Mukai T, Hayashi A, Iraha F, et al (2010) Codon reassignment in the Escherichia coli

genetic code. *Nucleic Acids Research* 38:8188–8195.

doi: 10.1093/nar/gkq707

27. Mukai T, Yanagisawa T, Ohtake K, et al (2011) Genetic-code evolution for protein synthesis with non-natural amino acids. *Biochemical and Biophysical Research Communications* 411:757–761.

doi: 10.1016/j.bbrc.2011.07.020

28. Isaacs FJ, Carr PA, Wang HH, et al (2011) Precise manipulation of chromosomes in vivo enables genome-wide codon replacement. *Science* 333:348–353.

doi: 10.1126/science.1205822

29. Johnson DBF, Xu J, Shen Z, et al (2011) RF1 knockout allows ribosomal incorporation of unnatural amino acids at multiple sites. *Nature Chemical Biology* 7:779–786.

doi: 10.1038/nchembio.657

30. Mukai T, Hoshi H, Ohtake K, et al (2015) Highly reproductive Escherichia coli cells with no specific assignment to the UAG codon. *Scientific Reports* 5:9699.

doi: 10.1038/srep09699

31. Hallam TJ, Wold E, Wahl A, Smider VV (2015) Antibody conjugates with unnatural amino acids. *Molecular Pharmaceutics* 12:1848–1862.

doi: 10.1021/acs.molpharmaceut.5b00082

32. Yanagisawa T, Umehara T, Sakamoto K, Yokoyama S (2014) Expanded genetic code technologies for incorporating modified lysine at multiple sites. *ChemBioChem: A European Journal of Chemical Biology* 15:2181–2187.

doi: 10.1002/cbic.201402266

33. Longstaff DG, Larue RC, Faust JE, et al (2007) A natural genetic code expansion

cassette enables transmissible biosynthesis and genetic encoding of pyrrolysine. *Proceedings of the National Academy of Sciences of the United States of America* 104:1021–1026.

doi: 10.1073/pnas.0610294104

34. Yanagisawa T, Ishii R, Fukunaga R, et al (2008) Multistep engineering of pyrrolysyl-tRNA synthetase to genetically encode Nε-(o-Azidobenzyloxycarbonyl) lysine for site-specific protein modification. *Chemistry & Biology* 15:1187–1197.

doi: 10.1016/j.chembiol.2008.10.004

35. Chin JW, Santoro SW, Martin AB, et al (2002) Addition of p-azido-l-phenylalanine to the genetic code of Escherichia coli. *Journal of the American Chemical Society* 124:9026–9027.

doi: 10.1021/ja027007w

36. Carell T, Vrabel M (2016) Bioorthogonal chemistry—introduction and overview. In: *Cycloadditions in bioorthogonal chemistry. Topics in Current Chemistry Collections* 374: 5–25.

doi: 10.1007/978-3-319-29686-9_2

37. Hendrickson TL, Crécy-Lagard VD, Schimmel P (2004) Incorporation of nonnatural amino acids into proteins. *Annual Review of Biochemistry* 73:147–176.

doi: 10.1146/annurev.biochem.73.012803.092429

38. Wang L, Xie J, Schultz PG (2006) Expanding the genetic code. *Annual Review of Biophysics and Biomolecular Structure* 35:225–249.

doi: 10.1146/annurev.biophys.35.101105.121507

39. Blight SK, Larue RC, Mahapatra A, et al (2004) Direct charging of tRNACUA with pyrrolysine in vitro and in vivo. *Nature* 431:333–335.

doi: 10.1038/nature02895

40. Polycarpo CR, Herring S, Bérubé A, et al (2006) Pyrrolysine analogues as substrates for pyrrolysyl-tRNA synthetase. *FEBS Letters* 580:6695–6700.
doi: 10.1016/j.febslet.2006.11.028
41. Chari RVJ (2016) Expanding the reach of antibody–drug conjugates. *ACS Medicinal Chemistry Letters* 7:974–976.
doi: 10.1021/acsmedchemlett.6b00312
42. Liu R, Wang RE, Wang F (2016) Antibody-drug conjugates for non-oncological indications. *Expert Opinion on Biological Therapy* 16:591–593.
doi: 10.1517/14712598.2016.1161753
43. Agarwal P, Bertozzi CR (2015) Site-specific antibody–drug conjugates: The nexus of bioorthogonal chemistry, protein engineering, and drug development. *Bioconjugate Chemistry* 26:176–192.
doi: 10.1021/bc5004982
44. Perez HL, Cardarelli PM, Deshpande S, et al (2014) Antibody–drug conjugates: current status and future directions. *Drug Discovery Today* 19:869–881.
doi: 10.1016/j.drudis.2013.11.004
45. Leung D, Wurst JM, Liu T, et al (2020) Antibody conjugates-recent advances and future innovations. *Antibodies* 9:2.
doi: 10.3390/antib9010002
46. Akekawatchai C, Holland JD, Kochetkova M, et al (2005) Transactivation of CXCR4 by the insulin-like growth factor-1 receptor (IGF-1R) in human MDA-MB-231 breast cancer epithelial cells. *Journal of Biological Chemistry* 280:39701–39708. doi: 10.1074/jbc.m509829200

47. Burtrum D, Zhu Z, Lu D, et al (2003) A fully human monoclonal antibody to the insulin-like growth factor I receptor blocks ligand-dependent signaling and inhibits human tumor growth in vivo. *Cancer Res* 63:8912–8921. doi:n.d.

48. Schanzer JM, Wartha K, Croasdale R, et al (2014) A novel glycoengineered bispecific antibody format for targeted inhibition of epidermal growth factor receptor (EGFR) and insulin-like growth factor receptor type I (IGF-1R) demonstrating unique molecular properties. *Journal of Biological Chemistry* 289:18693–18706.
doi: 10.1074/jbc.m113.528109

49. Kontermann R (2012) Dual targeting strategies with bispecific antibodies. *mAbs* 4:182–197.
doi: 10.4161/mabs.4.2.19000

50. Chen C, Zhang Y, Li J, et al (2014) Superior antitumor activity of a novel bispecific antibody cotargeting human epidermal growth factor receptor 2 and type I insulin-like growth factor receptor. *Molecular Cancer Therapeutics* 13:90–100. doi: 10.1158/1535-7163.mct-13-0558

51. Jin Q, Esteva FJ (2008) Cross-talk between the ErbB/HER family and the type I insulin-like growth factor receptor signaling pathway in breast cancer. *Journal of Mammary Gland Biology and Neoplasia* 13:485–498.
doi: 10.1007/s10911-008-9107-3

52. Nahta R, Yu D, Hung M-C, et al (2006) Mechanisms of disease: Understanding resistance to HER2-targeted therapy in human breast cancer. *Nature Clinical Practice Oncology* 3:269–280.
doi: 10.1038/ncponc0509

53. Gee JM, Robertson JF, Gutteridge E, et al (2005) Epidermal growth factor receptor/HER2/insulin-like growth factor receptor signalling and oestrogen receptor activity in clinical breast cancer. *Endocrine-Related Cancer* 12 (Suppl 1):S99–S111. doi: 10.1677/erc.1.01005

54. Chakraborty AK, Liang K, Digiovanna MP (2008) Co-targeting insulin-like growth factor I receptor and HER2: Dramatic effects of HER2 inhibitors on nonoverexpressing breast cancer. *Cancer Research* 68:1538–1545. doi: 10.1158/0008-5472.can-07-5935

55. Chakraborty AK, Zerillo C, Digiovanna MP (2015) In vitro and in vivo studies of the combination of IGF1R inhibitor figitumumab (CP-751,871) with HER2 inhibitors trastuzumab and neratinib. *Breast Cancer Research and Treatment* 152:533–544. doi: 10.1007/s10549-015-3504-2

56. Hutchins BM, Kazane SA, Staflin K, et al (2011) Site-specific coupling and sterically controlled formation of multimeric antibody Fab fragments with unnatural amino acids. *Journal of Molecular Biology* 406:595–603. doi: 10.1016/j.jmb.2011.01.011

57. Lyu Z, Kang L, Buuh ZY, et al (2018) A switchable site-specific antibody conjugate. *ACS Chemical Biology* 13:958–964. doi: 10.1021/acschembio.8b00107

58. Glazer AN (1970) Specific chemical modification of proteins. *Annual Review of Biochemistry* 39:101–130. doi: 10.1146/annurev.bi.39.070170.000533

59. Means GE, Feeney RE (1990) Chemical modifications of proteins: history and applications. *Bioconjugate Chemistry* 1:2–12.

doi: 10.1021/bc00001a001

60. Akla B, Broussas M, Loukili N, et al (2020) Efficacy of the antibody–drug conjugate W0101 in preclinical models of IGF-1 receptor overexpressing solid tumors. *Molecular Cancer Therapeutics* 19:168–177.
doi: 10.1158/1535-7163.mct-19-0219
61. Deonarain M, Yahioglu G, Stamati I, et al (2018) Small-format drug conjugates: A viable alternative to ADCs for solid tumours? *Antibodie*s 7:16.
doi: 10.3390/antib7020016
62. Lambert JM, Morris CQ (2017) Antibody–drug conjugates (ADCs) for personalized treatment of solid tumors: A review. *Advances in Therapy* 34:1015–1035.
doi: 10.1007/s12325-017-0519-6
63. Beckman RA, Weiner LM, Davis HM. (2007) Antibody constructs in cancer therapy: protein engineering strategies to improve exposure in solid tumors. *Cancer* 109:170-179.
doi: 10.1002/cncr.22402.
64. Richards DA (2018) Exploring alternative antibody scaffolds: Antibody fragments and antibody mimics for targeted drug delivery. *Drug Discovery Today. Technologies* 30:35–46.
doi: 10.1016/j.ddtec.2018.10.005
65. Deonarain MP (2018) Miniaturised 'antibody'-drug conjugates for solid tumours? *Drug Discovery Today. Technologies* 30:47–53.
doi: 10.1016/j.ddtec.2018.09.006
66. Li Z, Krippendorff B-F, Sharma S, et al (2016) Influence of molecular size on tissue distribution of antibody fragments. *mAbs* 8:113–119.

doi: 10.1080/19420862.2015.1111497

67. Uppal H, Doudement E, Mahapatra K, et al (2015) Potential mechanisms for thrombocytopenia development with trastuzumab emtansine (T-DM1). *Clinical Cancer Research: An Official Journal of the American Association for Cancer Research* 21:123–133.
doi: 10.1158/1078-0432.ccr-14-2093

68. Xenaki KT, Oliveira S, van Bergen En Henegouwen PMP (2017) Antibody or antibody fragments: Implications for molecular imaging and targeted therapy of solid tumors. *Frontiers in Immunology* 12:1287.
doi: 10.3389/fimmu.2017.01287

69. Badescu G, Bryant P, Bird M, et al (2014) Bridging disulfides for stable and defined antibody drug conjugates. *Bioconjugate Chemistry* 25:1124–1136.
doi: 10.1021/bc500148x.

70. Yu S, Pearson AD, Lim RK, et al (2016) Targeted delivery of an anti-inflammatory PDE4 inhibitor to immune cells via an antibody–drug conjugate. *Molecular Therapy: The Journal of the American Society of Gene Therapy* 24:2078–2089.
doi: 10.1038/mt.2016.175

71. Lim RKV, Yu S, Cheng B, et al (2015) Targeted delivery of LXR agonist using a site-specific antibody–drug conjugate. *Bioconjugate Chemistry* 26:2216–2222. doi: 10.1021/acs.bioconjchem.5b00203

72. Lehar SM, Pillow T, Xu M, et al (2015) Novel antibody–antibiotic conjugate eliminates intracellular S. aureus. *Nature* 527:323–328.
doi: 10.1038/nature16057.

73. Moek KL, Giesen D, Kok IC, et al (2017) Theranostics using antibodies and antibody-related therapeutics. *Journal of Nuclear Medicine: Official Publication, Society of Nuclear Medicine* 58 (Suppl 2):83S–90S.
doi: 10.2967/jnumed.116.186940

74. Zeglis BM, Davis CB, Aggeler R, et al (2013) Enzyme-mediated methodology for the site-specific radiolabeling of antibodies based on catalyst-free click chemistry. *Bioconjugate Chemistry* 24:1057–1067.
doi: 10.1021/bc400122c.

75. Zeglis BM, Davis CB, Abdel-Atti D, et al (2014) Chemoenzymatic strategy for the synthesis of site-specifically labeled immunoconjugates for multimodal PET and optical imaging. *Bioconjugate Chemistry* 25:2123–2128.
doi: 10.1021/bc500499h

76. Houghton JL, Zeglis BM, Abdel-Atti D, et al (2015) Site-specifically labeled CA19.9-targeted immunoconjugates for the PET, NIRF, and multimodal PET/NIRF imaging of pancreatic cancer. *Proceedings of the National Academy of Sciences of the United States of America* 112:15850–15855.
doi: 10.1073/pnas.1506542112

77. Kazane SA, Sok D, Cho EH, et al (2012) Site-specific DNA-antibody conjugates for specific and sensitive immuno-PCR. *Proceedings of the National Academy of Sciences of the United States of America* 109:3731–3736.
doi: 10.1073/pnas.1120682109

78. Chen S, Florinas S, Teitgen A, et al (2017) Controlled Fab installation onto polymeric micelle nanoparticles for tuned bioactivity. *Science and Technology of Advanced Materials* 18:666–680.

doi: 10.1080/14686996.2017.1370361

79. Hernandez K, Fernandez-Lafuente R (2011) Control of protein immobilization: Coupling immobilization and site-directed mutagenesis to improve biocatalyst or biosensor performance. *Enzyme and Microbial Technology* 48:107–122.
doi: 10.1016/j.enzmictec.2010.10.003
80. Nahta R, Yuan LX, Zhang B, et al (2005) Insulin-like growth factor-I receptor/human epidermal growth factor receptor 2 heterodimerization contributes to trastuzumab resistance of breast cancer cells. *Cancer Research* 65:11118–11128.
doi: 10.1158/0008-5472.can-04-3841
81. Browne B, Crown J, Venkatesan N, et al (2011) Inhibition of IGF1R activity enhances response to trastuzumab in HER-2-positive breast cancer cells. *Annals of Oncology: Official Journal of the European Society for Medical Oncology/ESMO* 22:68–73.
doi: 10.1093/annonc/mdq349
82. Scheer JM, Sandoval W, Elliott JM, et al (2012) Reorienting the Fab domains of trastuzumab results in potent HER2 activators. *PLoS ONE* 7:e51817.
doi: 10.1371/journal.pone.0051817
83. Georges GJ, Dengl S, Bujotzek A, et al (2020) The Contorsbody, an antibody format for agonism: Design, structure, and function. *Comput Struct Biotechnol J*. 2020;18:1210–1220.
doi:10.1016/j.csbj.2020.05.007
84. Kolumam G, Chen MZ, Tong R, et al (2015) Sustained brown fat stimulation and insulin sensitization by a humanized bispecific antibody agonist for fibroblast growth factor receptor 1/βKlotho complex. *EBioMedicine* 2:730–743.

doi: 10.1016/j.ebiom.2015.05.028

85. Coskun T, Bina HA, Schneider MA, et al (2008) Fibroblast growth factor 21 corrects obesity in mice. *Endocrinology* 149:6018–6027.
doi: 10.1210/en.2008-0816

86. Xu J, Stanislaus S, Chinookoswong N, et al (2009) Acute glucose-lowering and insulin-sensitizing action of FGF21 in insulin-resistant mouse models—association with liver and adipose tissue effects. *American Journal of Physiology-Endocrinology and Metabolism* 297:E1105–E1114.
doi: 10.1152/ajpendo.00348.2009

87. Arora, P. S. (2017) A bispecific agonistic antibody to FGF-R1/KlothoB improves the cardiometabolic profile in otherwise healthy obese subjects-preliminary results from the first-in-human single ascending dose study [abstract #1096]. Presented at the American Diabetes Association's 77th Scientific Sessions.

88. Janda CY, Dang LT, You C, et al (2017) Surrogate Wnt agonists that phenocopy canonical Wnt and β-catenin signalling. *Nature* 545:234–237.
doi: 10.1038/nature22306

89. Mohan K, Ueda G, Kim AR, et al (2019) Topological control of cytokine receptor signaling induces differential effects in hematopoiesis. *Science* 364:eaav7532.
doi: 10.1126/science.aav7532

90. Morris R, Kershaw NJ, Babon JJ (2018) The molecular details of cytokine signaling via the JAK/STAT pathway. *Protein Science: A Publication of the Protein Society* 27:1984–2009.
doi: 10.1002/pro.3519

91. Hercus TR, Kan WLT, Broughton SE, et al (2018) Role of the β common (βc) family of cytokines in health and disease *Cold Spring Harbor Perspectives in Biology* 10:a028514.
doi: 10.1101/cshperspect.a028514

92. Spolski R, Gromer D, Leonard WJ (2017) The γc family of cytokines: fine-tuning signals from IL-2 and IL-21 in the regulation of the immune response. *F1000Research* 6:1872.
doi: 10.12688/f1000research.12202.1

93. Stumpp MT, Dawson KM, Binz HK (2020) Beyond antibodies: The DARPin® drug platform. *BioDrugs: Clinical Immunotherapeutics, Biopharmaceuticals and Gene Therapy* 34:423–433.
doi: 10.1007/s40259-020-00429-8

94. Veri M-C, Burke S, Huang L, et al (2010) Therapeutic control of B-cell activation via recruitment of Fcγ receptor IIB (CD32B) inhibitory function with a novel bispecific antibody scaffold. *Arthritis and Rheumatism* 62:1933–1943.
doi: 10.1002/art.27477

95. Bachelet I, Munitz A, Levischaffer F (2006) Abrogation of allergic reactions by a bispecific antibody fragment linking IgE to CD300a. *Journal of Allergy and Clinical Immunology* 117:1314–1320.
doi: 10.1016/j.jaci.2006.04.031

96. Moraga I, Spangler JB, Mendoza JL, et al (2017) Synthekines are surrogate cytokine and growth factor agonists that compel signaling through non-natural receptor dimers. *eLife* 6:e22882.
doi: 10.7554/elife.22882

97. Krah S, Kolmar H, Becker S, Zielonka S (2018) Engineering IgG-like bispecific antibodies—an overview. *Antibodies* 7:28.
doi: 10.3390/antib7030028

8 Acknowledgments

九州大学大学院 薬学研究院 細胞生物学分野 田中嘉孝教授、石井祐次准教授、九州大学大学院 薬学研究院 生薬学分野 森元聡教授、坂元政一准教授、理化学研究所 生命機能科学研究センター 非天然アミノ酸技術研究チーム 坂本健作博士、大竹和正博士、理化学研究所 バトンゾーン研究推進プログラム 横山特別研究室 横山茂之博士、柳沢達男博士、協和キリン株式会社白石泰久氏、丹羽倫平氏はじめ、本研究をご指導・ご助言頂きました方々に心より感謝いたします。